universität wien

MASTERARBEIT/ MASTER'S THESIS

Titel der Masterarbeit / Title of the Master's Thesis

"Measuring hydrogeologic properties of unconsolidated sediments in unsaturated and saturated conditions using nuclear magnetic resonance"

Verfasst von/ submitted by
Ethan Jack Malone

angestrebter akademischer Grad / in partial fulfilment of the requirements for the degree of
Master of Science (MSc)

Wien, 2023 / Vienna, 2023

Studienkennzahl lt. Studienblatt / degree programme
code as it appears on the student record sheet: UA 066 680

Studienrichtung lt. Studienblatt / degree programme
as it appears on the student record sheet: Joint Master's Physics of the Earth

Betreut von / Supervisor: Ass.-Prof. Dr. Chi Zhang

Contents

Abstract

Subsurface imaging of the Earth has been performed for decades to acquire a range of geophysical data to help form a better understanding of our subsurface environment. In particular, the need to find, and manage groundwater sources is of critical importance. Measuring hydrogeologic properties of water in unconsolidated aquifers can be difficult, especially in unsaturated conditions (the vadose zone). In this thesis, borehole nuclear magnetic resonance (borehole NMR) measurements were performed using a newly acquired DART probe, from the company Vista Clara, to analyze numerous hydrogeologic properties in unsaturated and saturated sediment-water mixtures and compare the results to a rock analyzer which is a laboratory machine. The aim of this thesis was to examine the effect of saturation level, and particle size on the hydrogeologic properties of the sediment, and compare all of them. A pipe which represented a borehole was filled with different types of sediments in unsaturated and saturated conditions, in order to measure various hydrogeologic properties of these mixtures, such as the transverse relaxation time (T_2), pore-size distribution, estimates of hydraulic conductivity, and the water content. Then, the same sediment-water experiments at similar degrees of saturation were performed in a recently installed machine (rock analyzer) which performs NMR measurement, and measures T_2, which is compared to the experimental data from the DART probe, and the lab results from the rock analyzer. The sediments used in this research project were different types of gravel and sand which are the dominant materials in unconsolidated aquifers. It was found that the resulting hydrogeologic properties of different gravel/sand-water mixtures vary at different saturation levels, and the data from the DART probe and rock analyzer had different T_2 despite the experiments having similar degrees of saturation.

Kurzfassung

Seit Jahrzehnten werden unterirdische Bildaufnahmen der Erde durchgeführt, um eine Reihe geo-physikalischer Daten zu erfassen und so zu einem besseren Verständnis unserer unterirdischen Umwelt beizutragen. Insbesondere die Notwendigkeit, Grundwasserquellen zu finden und zu verwalten, ist von entscheidender Bedeutung. Die Messung der hydrogeologischen Eigenschaften von Wasser in nicht konsolidierten Grundwasserleitern kann schwierig sein, insbesondere unter ungesättigten Bedingungen (der Vadoszone). In dieser Arbeit wurden Kernspinresonanzmessungen (Bohrloch-NMR) mit einer neu erworbenen DART-Sonde der Firma Vista Clara durchgeführt, um zahlreiche hydrogeologische Eigenschaften in ungesättigten und gesättigten Sediment-Wasser-Mischungen zu analysieren und die Ergebnisse mit einem Gesteinsanalysator zu vergleichen ist eine Labormaschine. Das Ziel dieser Arbeit war es, den Einfluss des Sättigungsgrads und der Partikelgröße auf die hy-drogeologischen Eigenschaften des Sediments zu untersuchen und diese alle zu vergleichen. Ein Rohr, das ein Bohrloch darstellte, wurde mit verschiedenen Arten von Sedimenten in ungesättigtem und gesättigtem Zustand gefüllt, um verschiedene hydrogeologische Eigenschaften dieser Mischun-gen zu messen, wie z. B. die transversale Relaxationszeit (T_2), die Porengrößenverteilung und Schätzungen von hydraulische Leitfähigkeit und der Wassergehalt. Anschließend wurden dieselben Sediment-Wasser-Experimente bei ähnlichen Sättigungsgraden in einem kürzlich installierten Gerät (Gesteinsanalysator) durchgeführt, das NMR-Messungen durchführt und T_2 misst, das mit den exper-imentellen Daten der DART-Sonde verglichen wird Laborergebnisse vom Gesteinsanalysator. Bei den in diesem Forschungsprojekt verwendeten Sedimenten handelte es sich um verschiedene Arten von Kies und Sand, die in Lockergrundwasserleitern die vorherrschenden Materialien sind. Es wurde fest-gestellt, dass die resultierenden hydrogeologischen Eigenschaften verschiedener Kies-/Sand-Wasser-Mischungen bei unterschiedlichen Sättigungsniveaus variieren und die Daten der DART-Sonde und des Gesteinsanalysators unterschiedliche T_2 aufwiesen, obwohl die Experimente ähnliche Sättigungsgrade aufwiesen.

1   Introduction

The necessity for locating and management of groundwater in the Earth's subsurface is an ever growing important task [1]. For example, it's important to quantify how much water is stored in the subsurface of the Earth for ecosystems and water-rock interactions [2], as well as distinguishing groundwater from natural resources such as oil or gas. Different geophysical methods can be used to locate and visualize groundwater sources, such as seismology [3], and seismology can be useful in high alpine terrain areas which are difficult to access by foot. Other geophysical techniques that can be used are gravimetry and ground penetrating radar (GPR) [4], as well as electrical methods such as electrical resistivity tomography [5]. It is worth noting that some of the previous cited papers use combinations of the methods mentioned above which shows how the data sets can be combined to confirm the presence of groundwater as well transfer properties, for example GPR was used to measure the hydraulic conductivity of an unconsolidated aquifer [6]. Another method which can be used for detecting water in the subsurface of the Earth is nuclear magnetic resonance (NMR) which is the only non-invasive geophysical technique that collects the properties of the aquifer [7] [8], and this is the method used in this thesis. Not only can NMR locate water, but it can also measure various hydrogeologic properties such as pore-size distributions, types of water content, and the hydraulic conductivity (which is the rate at which water can flow through a rock or sediment in the vadose zone [9]) of rocks and geological material in the ground. Currently, NMR is the only method which can specifically measure water content and estimate its mobility in situ without using an active nuclear source [10] so this is another advantage to using NMR as a geophysical technique. NMR can be applied in unsaturated zones and saturated zones with the latter being the main focus of research when performing fieldwork. Hence, research in unsaturated conditions needs to be focused on. Another quantity of fluid-holding rocks is porosity, and combined with hydraulic conductivity, these values are needed to characterize seepage conditions (groundwater contamination in aquifers) and environmental problems [11]. Linking to this is the fact hydraulic conductivity controls water and pollutant movement [6], as well as water flow and nutrient cycling [12], so it can be inferred the importance of characterizing aquifers in the Earth's subsurface.

Mentioned in the abstract is a term called the 'vadose zone' which is the zone below the Earth's surface that contains unsaturated sediments and soil. The vadose zone is from the ground surface to the water table, which is the upper zone of the saturation zone within the Earth. While NMR measurements on water-saturated materials are well studied, there have only been a limited number of studies that focus on the interpretation of NMR measurements for applications in the vadose zone [13]. For example, estimating the hydraulic conductivity in unsaturated zones from empirical equations (such as Timur-Coates (TC) or Schlumberger Doll research (SDR)) and using data from NMR measurements requires that the saturated relaxation time be known. These equations also depend on empirically determined constants, which could limit the widespread application of this approach in the vadose zone [13]. Although no robust model has been developed that can be used to estimate vadose parameters, the direct relation between the initial signal amplitude and water content makes the NMR measurement useful for analysis of the vadose zone [13]. The aforementioned is a reason for experiments performed in this thesis because as a research community, we need a better understanding of unsaturated conditions of sediments from NMR data. Additionally, NMR can also be used for studies about the critical zone [14]. The critical zone is near-surface environment of the Earth which comprises of rock-water and organic material interactions and includes the vadose zone. This can affect the groundwater which is vital for humanity.

NMR isn't solely used for locating water, but it can be used for measurements of natural resources such as oil and gas. Within the petroleum industry NMR has been used to characterize fluid bearing porous materials [15] with focus on providing information on storage and transport properties of porous media [16] [17], and these properties could be permeability, pore sizes and types of fluids present [15]. Distinguishing between which fluids which are present in a porous medium based on the fluid properties is important, especially in the petroleum industry. Similarly, well logging has become important for characterizing subsurface properties for groundwater exploration and management, it is a great measurement technique because well logging is the means by which subsurface properties of the Earth are measured in-situ [18].

NMR was discovered in 1945 by 2 scientists, namely Felix Bloch, and Edwards Mills Purcell, and since then, the use of NMR has been enhanced. NMR is a great measurement technique because it can be performed in 3 ways. Namely laboratory NMR (lab NMR) i.e., a core analyzer in a laboratory, surface NMR (SNMR) performed on the Earth's surface, and finally borehole NMR which can extend to 10s or 100s of metres below the ground surface. Figure 1 shown below, which is self-made, summarizes each type of NMR and shows differences between the three types of NMR measurements. The first type of NMR method to be used was lab NMR, originally in the 1950s [18]. In 1969 Aytekin Timur first calculated the porous properties of different rocks in a laboratory, then used NMR to confer and compare the results [19]. In general, lab NMR is used to relate NMR properties to petrophysical parameters of interest. For example, a research group from Belgium used lab NMR to compare 4 different samples [20]. This is an advantage of lab NMR compared to SNMR and borehole NMR, in the sense that it allows multiple, different sediments to be measured one after the other or simultaneously which can lead to quick comparisons of data and observations of similarities and differences.

SNMR has become increasingly popular in the research community [21] which measures properties only in the very shallow structure at the Earth's subsurface. For example, this technique was used to measure hydraulic conductivity in the High Plains aquifer in the USA which is one of the most important in the world [22]. SNMR is different to lab NMR and borehole NMR, based on its principle and set up. On one hand, SNMR uses transmitter and receiver wire loops which measure the hydraulic properties of the subsurface, unlike borehole NMR where a probe is placed into the ground in a borehole to measure the hydraulic properties.

The final type of NMR method is borehole NMR, and this technique has been increasingly used in the field as the technology has increased. There are multiple studies that have used borehole NMR to measure groundwater as well as some porous properties [14] [23] [24]. Borehole NMR has been used frequently in industry to find oil, and measure water storage properties of different rocks and sediments deep in the subsurface of the earth in in-situ conditions. For example, borehole NMR can be used in the oil and gas industry to verify deposits and within the industry it's known as the 'eyes' of oil & gas exploration [25]. Borehole NMR uses the same principles as SNMR (a magnetic field and measuring the porous properties of the ground) but the depths at which borehole penetrates into the Earth is deeper than the depths of SNMR as implied by the names. A Borehole, which is a thin hole in the ground, extending vertically downwards below the Earth's surface, possibly up to hundreds of meters but also shallower depths. The diameter of a borehole is usually very thin. Hence, with borehole NMR, one can visualise a source of groundwater as well as which geological materials are present and what fluids they contain i.e., oil and/or water. In order to perform borehole NMR measurements, a probe is inserted into the borehole which can acquire the relevant geological data. An advantage of this method is that the probe can extend into the borehole and stop at regular intervals,

i.e., every 0.50 metres in order to acquire NMR data at all depths.

NMR	Inputs	Practical deployment	Measured NMR parameters	Limitations
Laboratory	• Capillary model • Viscosity • Density	• Used to determine NMR properties of materials • Relates petrophysical properties of NMR parameters to petrophysical relations	• Permeability • Hydraulic conductivity • Porosity • Vadose zone • Water retention curve	• Inhomogeneities in the magnetic field can affect the results.
Surface	• Earth's magnetic field (static field) • Excitation pulse	• Unlike other 2 methods, SNMR uses a wire loop • Earth's magnetic field is used • Measures amount of protons based on spin	• Subsurface water content is measured • Hydraulic conductivity • Estimate Pore structure of the studied formation	• Magnetic inhomogeneities. • Not as sensitive compared to BNMR
Borehole	• Borehole • Well depth height • # of averages • Scan length • Recovery time	• Measures water & hydrocarbon content in petroleum/ normal reservoirs • Slimline BNMR is used in near-surface environment. • Uses CPMG pulse	• Water content • Hydraulic conductivity • Pore size distribution • Relaxation time T_2	• Affected by magnetic properties of the mud. • Subjected to temperature/ pressure

Figure 1: A self-made image showing the three types of NMR with their inputs, and the different parameters they measure.

In this thesis, borehole NMR was performed in controlled conditions in a pipe which represented the borehole. Different gravel and sand sediments were mixed with water to form unsaturated and saturated mixtures which were examined by using a newly acquired DART probe from Vista Clara to measure various hydrogeologic properties. These properties measured by the DART probe are the transverse relaxation time T_2, pore-size distribution, hydraulic conductivity (K) and water content. Then, the same experiments were then performed in a newly acquired rock analyzer at similar saturation levels to compare the transverse relaxation time T_2 curves to the T_2 spectra from the experimental borehole NMR data. Also, estimates of total water content [grams] were derived from the signal amplitude of the T_2 measurements from the rock analyzer. The aim of this thesis is to compare the two different data sets between sediment-water mixtures in unsaturated and saturated conditions, and see if particle size and saturation level affect the hydrogeologic properties mentioned above. as well as observing the functionality of the DART probe. Unconsolidated aquifers provide a challenge in the field since they contain intergranluar grains [26], so porosity values and hydraulic conductivity can be affected by the materials in unconsolidated aquifers. Sand and gravel constitute a major geological formation in unconsolidated aquifers. These are the sediments measured in this thesis, so the results from this thesis can be combined with results from research from the field to gain a better understanding of hydrogeologic properties in unconsolidated aquifers, for example in the United States of America where there are many unconsolidated aquifers [26]. Also, materials in unconsolidated aquifers have shown that the relationship between NMR data and the pore geometry is poorly understood [27], hence the measurements performed in this thesis can help contribute to this knowledge gap by analysing NMR data sets from the DART probe and rock analyzer. The next section of this thesis describes the theory and principles behind NMR measurements, followed by the experimental procedure carried out to get the results in the this thesis. Finally, the results are

presented and discussed accompanied by concluding remarks and an outlook for future research.

2   Theoretical background

2.1   Nuclear magnetic resonance (NMR)

For the reference of the reader, some of the theory described in this section was assisted with the book ' NMR principles logging and applications' [35], which is a good book to read if one would like to delve deeper into the science of NMR.

In order to detect the presence, and volume of water in porous media or geological structure such as a borehole, nuclear magnetic resonance (NMR) essentially measures the amount of hydrogen present. More precisely, NMR measures the response of atomic nuclei to magnetic fields and since water is the fluid used in this thesis, the discussion will focus on water. For reference, the chemical formula of water is H_2O, and one hydrogen atom consists of one proton. Hence, NMR uses the protons in the water to measure the amount of water, and then based on the NMR signal the hydrogeologic properties of the medium can be determined (such as hydraulic conductivity and pore-size distribution). For borehole NMR, a probe is needed to measure the water content surrounding the borehole. In this thesis, the probe used was a DART probe, from the company Vista Clara. An example of what a Javelin probe looks like in a real borehole is shown in figure 2, which is taken from [13] and [23], and one can see the measurement region extends to outside of the borehole. Even though the Javelin probe is not the DART probe, they both measure similar properties and the operation is also similar.
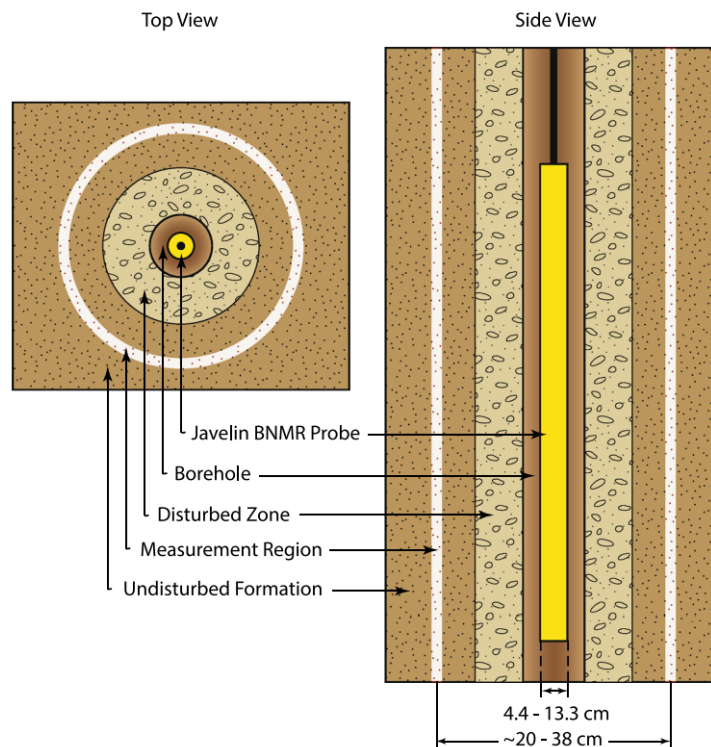

Figure 2: A side and bird's eye view of a Javelin probe in a borehole. Image adapted from [13] and [23].

For the application of a DART probe, a proton can be considered as a small, charged sphere which has a magnetic dipole moment (M_p) and intrinsic spin angular momentum (I_p). The ratio of M_p to

I_p is called the gyromagnetic ratio $\gamma_p = M_p / I_p$, which is related to the Larmor frequency f shown in equation 1:

$$f = \gamma_p * B_0 / 2\pi$$

Where:

f = Larmor frequency [Hertz]
γ_p= Gyromagnetic ratio [radian/(Second*Tesla)]
B_0 = Static magnetic field [Tesla]

I.e., the Larmor frequency links the precession of a proton around the axis of a magnetic field, which will be explained shortly.

Without any applied magnetic field to a porous medium, a proton will lie in the lowest energy level state within the hydrogen atom, and it can not move to another state. For NMR measurements performed in a borehole, a static magnetic field (B_0 in equation 1) is generated from the DART probe, and applied to the borehole which polarizes the proton's spins into an equilibrium state. This produces a (small) net magnetization which is parallel to the axis of the applied static magnetic field (longitudinal plane). This leads to precession of the protons around the magnetic field, at the precessional frequency (larmor frequency). In order to observe an NMR signal that is measurable, the polarised spins of the protons need to be perturbed from their equilibrium state. Therefore, the second step to produce an NMR signal is to apply a pulsed magnetic field (called CPMG named after the its inventors Carr, Purcell, Meiboom and Gill) which acts in the form of a radio frequency (RF) pulse, and it is tuned to the larmor frequency. This RF pulse is applied in the transverse plane (the plane perpendicular to the static magnetic field) which acts effectively like a torque. This causes the net magnetization to rotate from the longitudinal plane, into the transverse plane which is a higher energy state. The initial amplitude of the magnetization is directly proportional to the volume of hydrogen. After the application of the RF oscillating field ceases, the transverse magnetization component precesses around the static magnetic field axis. This precession of the transverse magnetization leads to a detectable signal that oscillates at the larmor frequency. After the RF pulses are ceased, the spins of the protons gradually relax back to their equilibrium state, leading to a decay of the observed NMR signal, and this decay of the transverse magnetization is the transverse relaxation time T_2. The de-phasing of the proton spins from their transverse plane back to their equilibrium position leads to the spin relaxation time being measured. In reality multiple CPMG pulses are applied, and the time between each pulse is a inter-echo spacing (time between each individual spin echoes).
The transverse relaxation time T_2 is measured and used in this thesis since the transverse relaxation time T_2 contains most of the petrophysical information about the rock [35]. Also, T_2 can inform one about the pore-scale environments of the spins of the protons and it can be used to derive estimates of pore size.

The spin-echoes are measured by the DART probe and these constitute the raw NMR data [35].
The number of hydrogen nuclei (and hence number of protons) in a volume of fluid in a pore space relates to the initial amplitude of the spin-echo train. The T_2 relaxation time affects the spin-echo train. The inter-echo spacing, and polarization time (beginning of measurement of the next echo train) are

data acquisition parameters for the overall spin-echo train.

As mentioned before, The transverse relaxation time T_2 is measured in this thesis, and T_2 is given by equation 2:

$$T_2 = 1/T_{2b} + 1/T_{2s} + 1/T_{2d}$$

Where:

T_{2b} = Bulk transversal relaxation time
T_{2s} = Surface transversal relaxation time
T_{2d} = Diffusion transversal relaxation time

T_{2b} is the relaxation time measured when wall and gradient effects are not present [38], i.e., T_{2b} is an intrinsic property of a fluid [35]. T_{2s} is the relaxation resulting from the pore wall [38] which can sometimes affect the data. T_{2d} is the relaxation component that is shortened by molecular diffusion in an inhomogeneous static magnetic field [38]. For the interpretation of the T_2 relaxation time usually relies on the assumption that, if the diffusion between a proton and other pores is limited (so no pore-coupling effects), then diffusion occurs in the fast regime and the surface relaxivity is uniform throughout the measured volume [36]. It should be noted for the fast diffusion limit, T_{2d} time can be ignored because the inter-echo spacings are short. Fast diffusion condition is where the diffusion of the hydrogen nuclei within the pore space is not the rate controlling step in the relaxation process [22], and the fast diffusion regime is an assumption made, to better interpret the NMR data [36]. Another assumption made is the surface relaxivity is constant throughout the measured volume [36] which means there should be a linear relationship between T_2 and the pore size distribution.

Another property that the DART probe can measure is the hydraulic conductivity (K), and the hydraulic conductivity is the ability of a soil or rock to transmit water i.e, how easily does water flow through a sediment. K can be determined using different models, for example Schlumberger-Doll research (SDR) model or Timur-Coates (TC) model. Both models require that relaxation occurs in a fast diffusion regime [13]. The DART probe estimates K using the SDR, TC and SOE (sum of echoes) empirical equations, and these are not calculated by myself. These equations rely on constants from consolidated materials (usually sandstones) but there is continuous research in the field to modify and improve the values of these constants. Hence, the diffusion transversal relaxation time T_{2d} can be ignored for the experiments performed in this thesis since the estimates used for K require the fast diffusion regime [13].

As mentioned before, the DART probe also measures estimates of water content with depth of the borehole. The three types of water which are measured by the DART probe are: Clay-bound water (CBW), Bound water (BVI) which is also known as capillary water, and mobile water (BVM). CBW is usually defined as water within the clay lattice of a rock, or water near the surface of the electrical double layer (EDL) [33], but The signal amplitude from water in clay-bound pores can decay very quickly (smaller pores) [10]. BVI can be defined as a very thin layer of water that covers the surrounding mineral surfaces [34], and this thin layer of water is less mobile than the rest of the water in the sediment. An assumption is that BVI resides in small pores [35], but the signal amplitude from water in capillary-bound (bound water) pores decays quickly [10]. Combined with this statement is

that bound water can also be defined as water contained in the pore that will not flow out of the rock [35]. The water regimes are separated by standard cut off times which are derived from oil reservoir sandstones [23]. The standards are usually: CBW = $T_2 < 3$ ms, BVI = 3 ms $< T_2 <$ 33 ms, and BVM = 33 ms $< T_2$, and these were used for this thesis.

2.2   Inverse modelling

Inverse modelling is the method needed for producing models from NMR data An inverse problem is described by the input and data, which are the given parameters to a problem, but the 'model' space is unknown. Typically the forward problem is modelled as shown in equation 3:

$$G(m) = M * d$$

Where:

G(m)= Input
M= Model space
d= Data

Usually, the forward problem is unique (has one solution) but the inverse problem is non-unique. So, the inverse problem is to determine the model space using the input and data, which is the require modelling technique needed for borehole NMR because one can get the model of the hydrogeologic properties of a rock/sediment using the data obtained.

The inverse modelling software of NUCLEUS, called NUCLEUSinv was the software used for this thesis to invert the data and produce the T_2 and pore-size distribution curves [30]. NUCLEUS is a free, open source inversion program created by Dr. Thomas Hiller. An image of the NUCLEUSinv interface can be found in appendix D along with information about the workflow and execution of NUCLEUSinv. The raw data from the DART probe is outputted in the form of a 'mat-file', and this is the input for NUCLEUSinv. There are different techniques which can be used for inverting the data, such as the 'several free exponents' method or the 'Multi exponents least squares' (LSQ) method, which was the inversion process used in this thesis. The LSQ method fits the curve by adjustment of a range of exponential functions. The LSQ method is used in regression analysis to approximate the solution of a inverse problem, and the LSQ method minimizes the residuals of the data in order to produce a better fit. For an inverse problem the residual is the difference of a modelled value and an observed value from an experiment. In the LSQ method, a regularization parameter is determined which is commonly known as lambda (λ), and for each data point there is a λ value. When all the λ values are plotted together, it forms an 'L-curve' which symbolizes the norm of the regularized solution vs the norm of the residual.

2.3   Current challenges with NMR

As with every scientific method, there can always be some problems or errors that need to be taken into account. For example, with borehole NMR one problem which has to be overcome is the pres-

ence of magnetic gradients within the material being measured as found by Flinchum et al [14]. The magnetic gradients causes the protons to oscillate at different larmor frequencies, and this variation in larmor frequency creates a more rapid decay signal [14]. Linking to this is the presence of certain minerals in a material, for example, iron minerals (which are magnetic) can also cause the protons to diphase during relaxation which could lead to a more rapid decay signal and reduced T_2 relaxation time [14]. The last two sentences indicate how the influence of iron can benefit negatively affect NMR measurements. As well as this, the magnetic field is weaker when using borehole NMR compared to lab NMR because in borehole NMR the rock/sediment is outside of the source [10], as can be seen in figure 2, and this also means the magnetic field can vary more throughout the sample volume [10]. Linking to this, is the fact that the static magnetic field used in borehole NMR is highly inhomogeneous [13], especially the greater the radius the probe is from the borehole. Another problem with NMR could be pore coupling effects which have been mentioned briefly. Previously, simulation of pore coupling effects in pores has been performed and investigated [41]. Pore coupling involves inter-connected pores within a rock or sediment which allows hydrogen atoms to diffuse from one more space to another within an NMR measurement [41]. This makes interpreting NMR data more difficult because conventionally, it is assumed that one hydrogen atom i.e., one proton corresponds to one pore space.

3   Experimental procedure

This thesis comprises of data sets from two apparatus, one data set is from a DART probe which was used to perform borehole NMR measurements, and the other data set was obtained from a rock analyzer. First the experimental method for the DART probe will be discussed, followed by the procedure for the rock analyzer. Then, the sediments that were used are stated and shown, followed by a description of the NUCLEUISinv inversion program used to produce the transverse relaxation curves and pore size distribution curves. Figure 3 is a table self-made image with assistance from [28], that shows the relative advantages of using a Javelin probe logging cable to measure fluid properties rather than other geophysical methods, to emphasize why a DART probe is better in borehole NMR than other NMR methods. It can be noticed in figure 3 that it refers to a Javelin probe, and not the DART probe. Although the Javelin cable is not the exact probe used in this thesis, it is very similar to the DART probe which was used, and they're both produced by the company Vista Clara.From looking at figure 3 it can be seen overall that the javelin probe is the overall best probe to use for borehole measurements in terms of data collection compared to other methods.

Characterization method	Javelin NMR probe (Vista Clara)	Well drilling	Other Geophysical logging	Laboratory analysis
Relative cost	€€	€€€€€€€€	€	€€€€€
Continuous data	🟩	🟩	🟩	🟥
Pore size distribution	🟩	🟥	🟥	??
Hydraulic conductivity	🟩	🟥	🟥	🟩
Bound/Mobile porosity	🟩	🟥	🟥	🟩
Total porosity	🟩	🟥	🟥	🟩

Figure 3: A self made image showing the relative advantages of the DART probe used for borehole NMR compared to other geophysical methods. Adapted from [28].

3.1   Borehole NMR

The DART probe allows the following properties of a rock to be measured using computer software: Clay, bound and mobile water content, hydraulic conductivity (K), and the pore size within the porous medium using the transverse relaxation time T_2. The DART probe produced by Vista Clara is the only portable probe worldwide available which can be deployed easily in the field [28]. Only a control unit, battery, laptop and a few cables (shown in figures 4 and 5) are needed in order to obtain the raw data which can then be processed. The way the DART probe measures the water content in a borehole is by performing one or more 'stages' at a given depth level. Each stage is composed of 'scans' at different frequencies, and then a scan is repeated to form multiple averages. The factors that vary between each stage is the time between each measurement average T_r, and the length of each scan (which is the length of each CPMG measurement) [29].

Figure 4 shows the DART probe in a bucket of water for the reader's reference to see how it appears. In order to set up the DART probe a number of steps had to executed. Firstly, the DART probe was connected to the logging cable, which is the black cable shown in figure 4a. Next, the control unit was set up and all relevant cables were connected. It can be seen in figure 5 that there are multiple ports, and these are where each cable was connected. Going from left to right in figure 5, the first port connects the power supply to the control unit (in this experiment the power supply was a 12 V battery). The port next to this is a REF port, this is optional and was not used during this thesis. The third port is the SENSOR port which connects the logging cable to the control unit, and thus allows power to be provided to the DART probe. The final port on the far right is the USB connection which allows a field computer to be connected, in order to visualize live data accumulating during data collection. When data collection begins, the user sees the interface as shown in figure 6. This is the software from Vista Clara, as well as the software used for initial data processing. This is where the user can set parameters such as scan length, and the inter echo time, which are related by equation 4:

$$(f * Scan)/T_r \leq 0.2$$

Where:

f = Number of frequencies (for the DART probe, f = 2)
Scan = Scan length [Seconds]
T_r = Recovery time [Seconds]

In order to avoid errors, Vista Clara suggest to set up the parameters so that they obey this equation [28].

The two frequencies are F_1 & F_2 (with $F_1 > F_2$). F_1 only measures water which recovers within a small vicinity of the probe after each RF pulse, where as frequency F_2 will measure all recovered water. T_r controls the amount of time between successive CPMG measurement scans at a certain frequency. Essentially, T_r determines the length of time allowed for the formation of recovery between measurements. A long T_r value means all water in the geological formation will be detected since all the water in the formation will be allowed to recover, where as a short T_r value means only water with a short relaxation time will be measured accurately.

Before performing an experiment and beginning data collection, the frequencies of the DART probe had to be checked (calibrated), in order to get an estimate of the background noise. This can be useful when performing data analysis and interpreting the data so that one can cancel out background noise. Once this was completed, data collection could begin. As can be seen on the the interface in figure 6, there are 2 channels on the upper right of the software interface. The topmost channel corresponds to each successive individual CPMG measurement, whilst the channel below that shows an average of all successive CPMG measurements. The two Gaussian shaped peaks towards the bottom left of figure 6 show the two frequencies (F_1 & F_2) which are used by the DART probe to pulse the protons out of their equilibrium position. The manual advised not to alter any advanced sequence settings of this software unless one was experienced with the software [29], and since this was my first time using this apparatus, the advanced sequence parameters were not changed so all data was accumulated

(a) The DART probe in a bucket of water
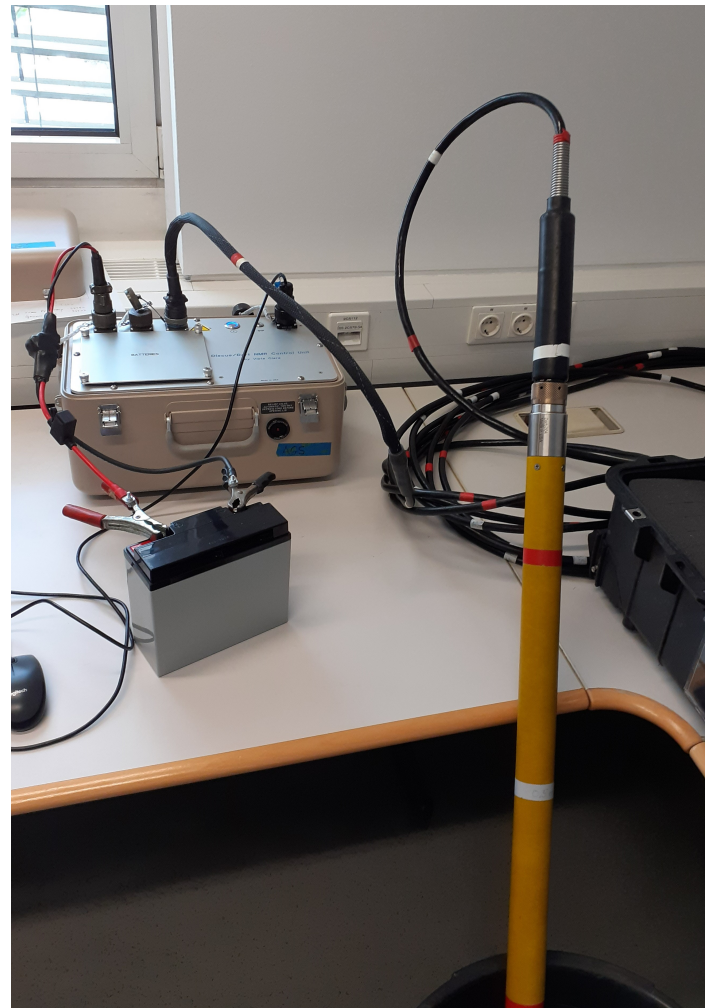
(b) The DART probe connected to the control unit via the logging cable, ready for data collection

Figure 4: Images showing the DART probe from Vista Clara and how it is connected to the control unit.

using the pre-set acquisition settings.

Once all the above steps had been completed, the experiment could begin. For the borehole NMR experiments, a pipe was used which in controlled conditions was the borehole, and an image of the borehole can be found in appendix C. The borehole was filled with a sediments at the desired saturation level, up to a height of 0.500 ± 0.001 m. The bottom of the pipe was enclosed by a cap so that no sediment could escape, although in some experiments small quantities of sediment such as sand leaked out but this was taken into consideration. Unsaturated and saturated sediment-water mixtures were created and then the DART probe was inserted into the pipe, and measurements could begin, as described above. Specific types of each sediment used are stated below in the 'sediments' subsection. For each experiment, the dry mass of each sediment used was 7.500 ± 0.0005 kg. Then based on the desired saturation level, the correct amount of water was added to make the sediment-water mixture a certain wet mass. The wet masses were calculated using values of the specific gravity for each sediment, combined with equations for calculating the required wet mass to make the sediment-water

Figure 5: The control unit which provides power to, and controls the DART probe.
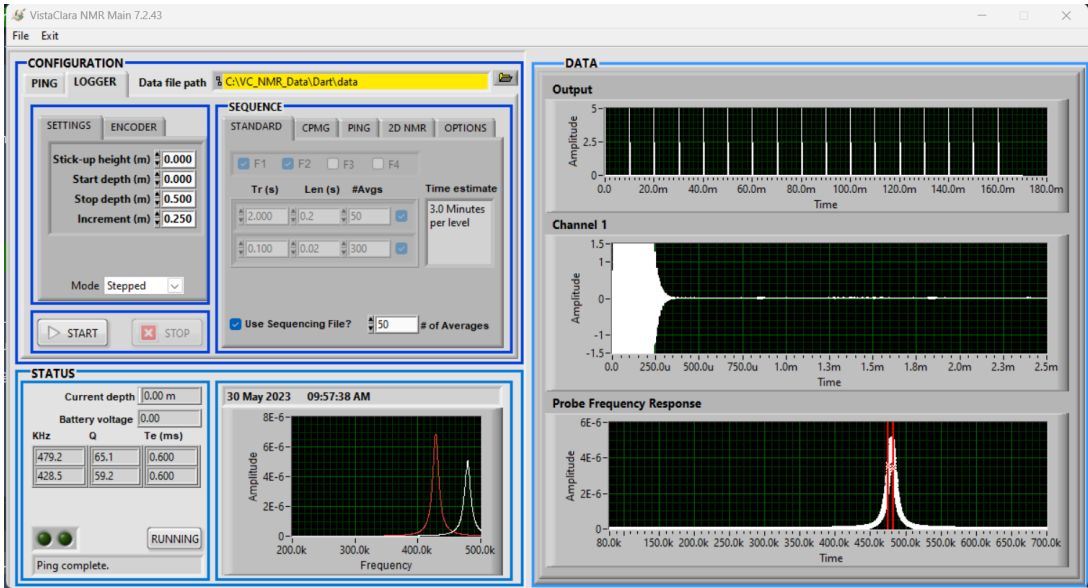

Figure 6: The software used during data acquisition when using the DART probe.

mixture a desired level of saturation. The precise quantities of dry mass and wet mass used of each sediment used for the borehole measurements are listed in appendix A. The three degrees of saturation that were measured were S_r = 0.100, 0.500 and 1.000, so a range of saturation levels were tested from very low saturated (S_r = 0.100), to medium saturated (S_r = 0.500), and to fully saturated (S_r = 1.000). In reality, the degree of saturation of the sediment-water mixtures for each experiment was not exactly 0.100,0.500 or 1.000 i.e., $S_r \approx$ 0.100/0.500/1.000, due to measurement error but the real values were in close proximity to these. Since the borehole was experimental, the set up was not exactly like the javellin probe in figure 2. This is important to consider, and it should be noted that during the experiments using the DART probe, the whole DART probe was not not surrounded by the sediment. Hence, this could explain some of the patterns seen in the data, especially the decay curves (as will be seen).

3.2   Rock analyzer

In order for measurements to be performed in the rock analyzer, which is shown in figure 7, the sample of the sediment used (at the desired saturation level) was placed into the core holder and then sealed by a lid. As can be seen from the images in figure 7, the sample holder was small (the diameter was 3.81 cm and height 10.0 cm). Hence, the dry & wet masses of the sediment used in the rock analyzer were smaller than the dry & wet mass of the sediment used in the borehole experiments. For every experiment performed using the rock analyzer, a smaller initial dry mass was used compared to the mass of the dry masses used in the experiments for the borehole. Despite much smaller dry and wet masses being used in the rock analyzer, the degree of saturation of the sediment-water mixtures were approximately kept the same ($S_r \approx$ 0.100/0.500/1.000) in order to ensure a fair test and comparison for the transverse (T_2) relaxation curves. Once the unsaturated/saturated sediment was in the sample holder and sealed with the lid, the sample holder was then placed into the core holder of the rock analyzer and measurements could begin.

3.3   Sediments

Six different types of sediments were used in this thesis, namely three types of gravel were used, namely crushed marble stone, round/quartz gravel and lawn quartz. As well as three types of sand, namely joint sand, lawn sand and quartz sand. Then, these sediments were combined with water to form a partial or fully saturated mixture. The gravel sediments used in this thesis, along with their particle size are shown below in table 1, and the sand sediments used in this thesis, along with their particle size are shown in table 2.

Table 3 below shows the calculated porosity value of each substance used for the borehole NMR experiments on a 0 to 100 % scale. The values were calculated by myself based on the quantity of each sediment used. Porosity relates the volume of the voids i.e., the empty space to the total volume of a material. The equation for porosity is give by equation 9:

$$\phi = V_V / V_T$$

ϕ = Porosity [%]
V_V = Volume of the pores [m^3]

Figure 7: Clockwise from top left: rock analyzer used for lab NMR from the company 'Niumag corporation' based in China, core holder, sample holder sealed and unsealed with a lid which is where the sample is placed into.

V_T = Total volume [m^3]

Degree of saturation S_r / Material	Marble	Rundkies	Rasenquarz	Fugensand	Rasensand	Quartzsand
≈ 0.100	95.2 ± 1.4	94.5 ± 1.4	93.2 ± 1.4	95.6 ± 1.4	96.3 ± 1.5	96.0 ± 1.5
≈ 0.500	77.0 ± 1.2	74.3 ± 1.1	70.9 ± 1.1	82.4 ± 1.2	82.4 ± 1.2	82.4 ± 1.2
≈ 1.000	54.2 ± 0.8	48.6 ± 0.7	43.0 ± 0.6	64.4 ± 1.0	64.8 ± 1.0	64.9 ± 1.0

Table 4 below shows the calculated porosity value of each substance used for the rock analyzer experiments on a 0 to 100 % scale. The values were calculated by myself based on the quantity of each sediment used. Porosity relates the volume of the voids i.e., the empty space to the total volume of a material. The equation for porosity is give by equation 9:

Saturation level S_r / Material	Crushed Marble	Round gravel	Lawn quartz	Joint sand	lawn sand	Quartz sand
≈ 0.100	97.1 ± 1.5	97.2 ± 1.5	96.8 ± 1.5	97.0 ± 1.5	97.3 ± 1.5	97.2 ± 1.5
≈ 0.500	86.1 ± 1.3	86.1 ± 1.3	86.2 ± 1.3	87.5 ± 1.3	87.5 ± 1.3	87.5 ± 1.3
≈ 1.000	72.4 ± 1.1	72.2 ± 1.1	73.0 ± 1.1	74.5 ± 1.1	75.0 ± 1.1	75.1 ± 1.1

3.3.1   Gravel

Marble (4-8 mm)	Round/Quartz gravel (4-8 mm)	Lawn quartz (0.5-2.0 mm)

Table 1 above shows photos of each gravel sediment used in this thesis with the particle size of each sediment. It can be seen from table 1 that the lawn quartz used in this thesis, had considerably smaller particles than the crushed marble and round/quartz gravel. Thus, the effect of particle size could be analyzed when interpreting the data of the hydrogeologic properties for the gravel-water mixture experiments for the borehole and rock analyzer.

3.3.2   Sand

Joint sand (0.1-0-3 mm)	Lawn sand (0.06-2.00 mm)	Quartz sand (0.06-0.30mm)

Table 2 above shows photos of each sand sediment used in this thesis with the particle size of each type of sand. It can be seen from table 2 that the lawn sand used in this thesis, had some considerably bigger particles than the joint sand and quartz sand. Thus, the effect of particle size could be analyzed when interpreting the data of the hydrogeologic properties for the sand-water mixture experiments for the borehole and rock analyzer.

3.4   Data processing

Data analysis had to be performed in order to visualise, and interpret the data that was accumulated from the experiments. As mentioned before, the graphs relating signal amplitudes and transverse relaxation time T_2 were produced by using a free online software called NUCLEUS which operates through a MATLAB terminal [30]. [13]. NUCLEUS stands for: modelling and iNversion of nUCLear magnetic rEsonance data with angUlar poreS.

NUCLEUS is an open source program created by Dr.Thomas Hiller which can be used for the inversion and modelling of raw NMR data [30]. Before the data was uploaded to NUCLEUSinv, basic data analysis was performed with the Javelin program provided by Vista Clara. This stage involved removing noise (if there was any present) and also producing the initial estimates of water content and hydraulic conductivity. The data analysis program which was used for the DART probe produces a mat-file which was then uploaded to MATLAB, and thus, into the NUCLEUSinv program as well. Appendices C and D contain information about using the DART probe, the data processing software and the NUCLEUSinv program. The final graphs produced from the NUCLEUSinv software are the amplitudes of the spin-echoes vs transverse relaxation time T_2, and the amplitudes of the spin-echoes vs pore-size distribution. The graphs produced lead to observations and conclusions about the geological structure measured such as the pore environment. The data regarding the hydraulic conductivity and water content estimates was automatically processed by the data processing software required to be used with the DART probe, and no other program was needed to produce this data.

.

4   Results

The results section is split into subsections for each saturation level with data for the T_2 relaxation time from the borehole NMR and rock analyzer experiments, pore-size distribution from the saturated borehole NMR experiments. The saturated data is presented first, then the unsaturated conditions in descending order. Within each saturation subsection there are two subsubsections which present the results for the gravel materials, and the sand materials. These data sets are followed by two more subsections which discuss a summary of the hydraulic conductivity & water content estimates from the DART probe, and the derived water content from the rock analyzer.

4.1   Saturation level $S_r \approx 1.000$

4.1.1   Gravel
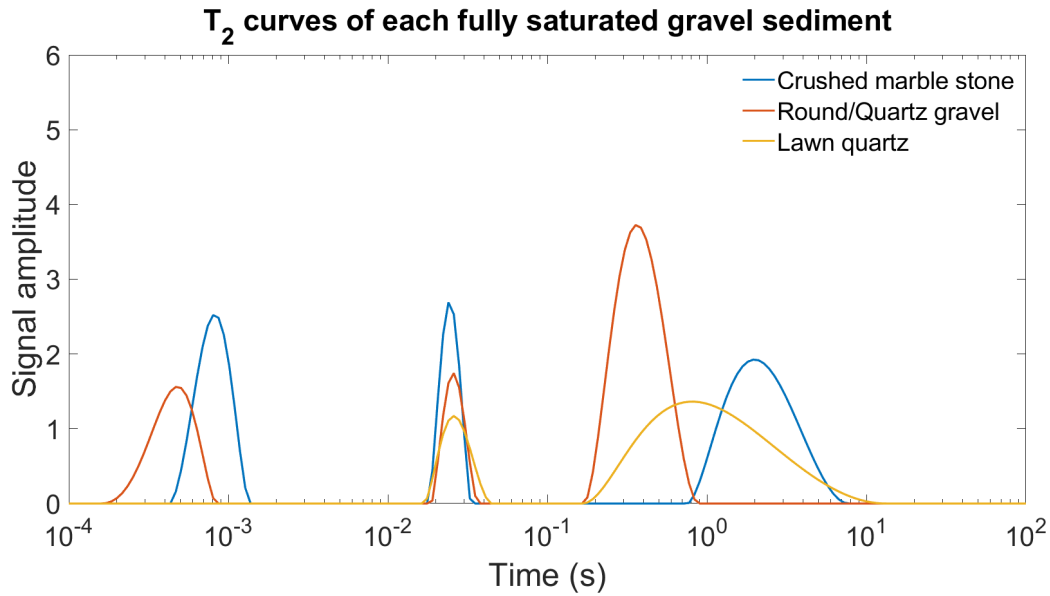
(a) T_2 relaxation times from three borehole NMR experiments using fully saturated gravel-water mixtures.
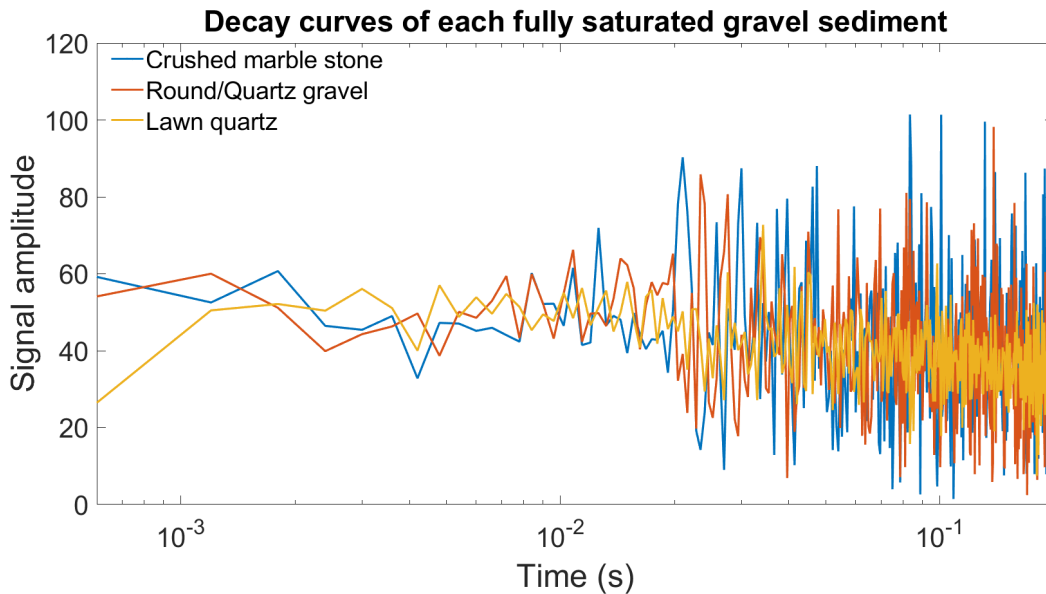
(b) Spin echo decay curves in three fully saturated gravel-water mixtures.

Figure 8: Graphs showing the T_2 relaxation and decay curves of fully saturated gravel-water mixtures with data obtained from borehole NMR experiments. The exact degree of saturation for each sediment can be found in appendix A.1.

Figure 8 shows the T_2 and decay curves relating to signal magnitude for each saturated gravel-water mixture from borehole NMR. All the gravel sediments exhibited similar relaxation times at larger and smaller T_2 values. Except lawn quartz which did not show any transverse relaxation at lower T_2 values. Particularly at a T_2 value in the range of 10^{-2}-10^{-1} seconds, the three gravel sediments had a curve at the same point. It can also be seen in figure 8a that every curve for each gravel sediment was

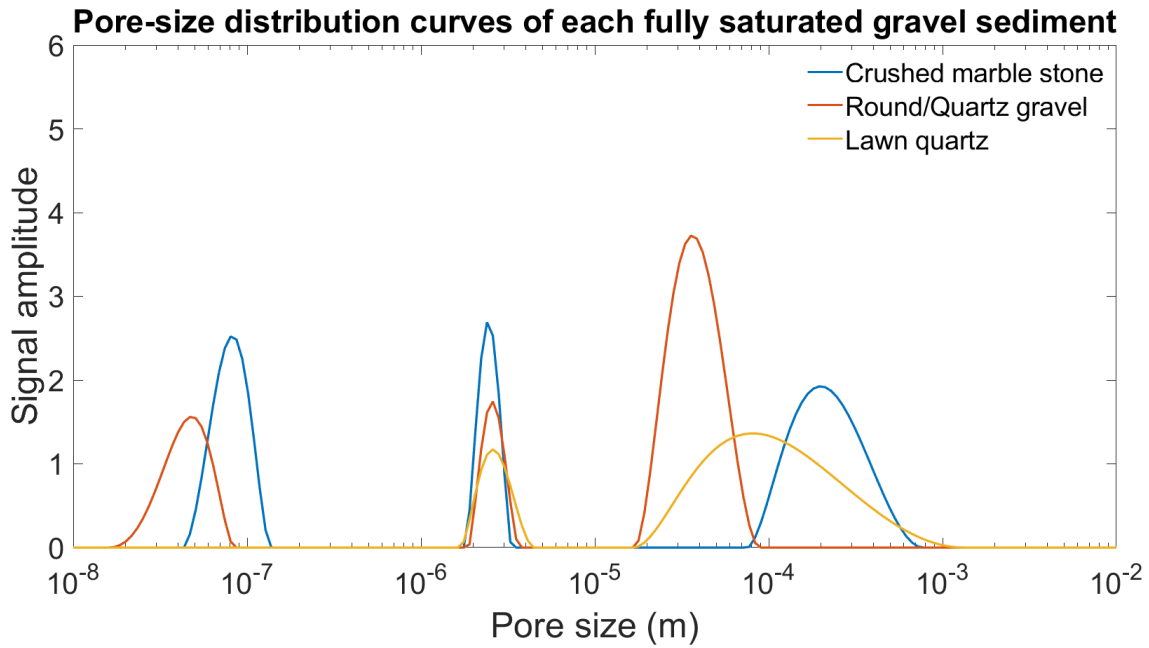Figure 9: Pore-size distribution curves of fully saturated gravel-water mixtures with data obtained from borehole NMR experiments. The exact degree of saturation for each sediment can be found in appendix A.1.
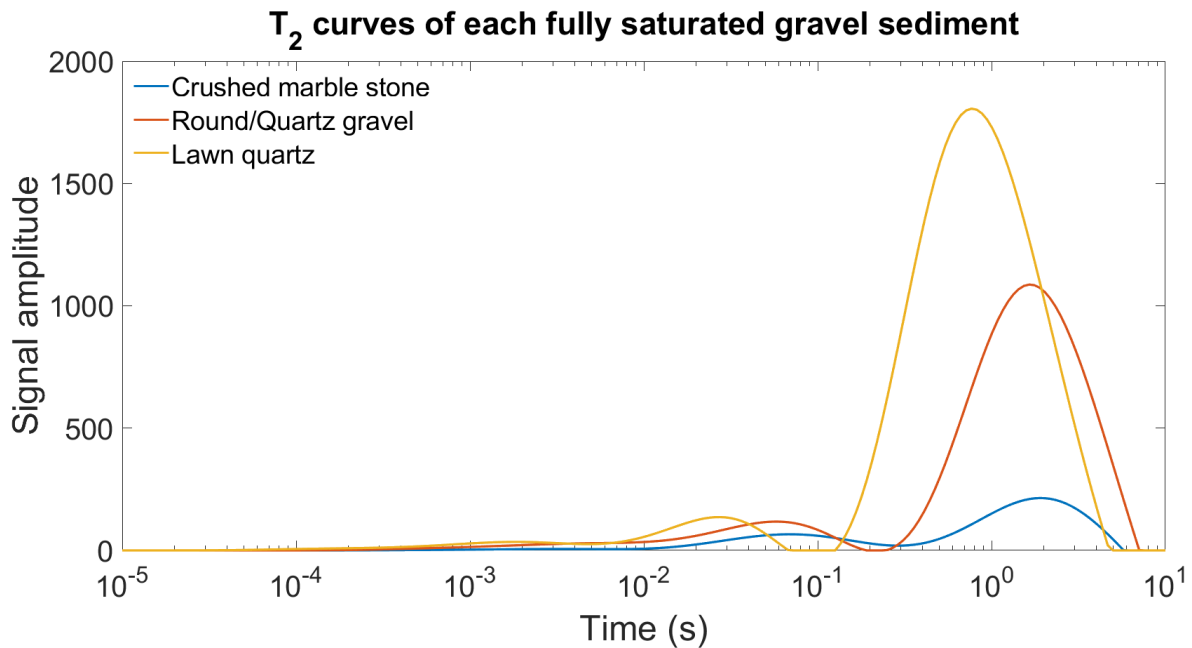

Figure 10: T_2 relaxation curves of fully saturated gravel-water mixtures with data obtained from rock analyzer experiments. The exact degree of saturation for each sediment can be found in appendix B.1.

separate, and not joined with another i.e., each curve increases from a signal magnitude of 0, reaches a peak value, and then decreases back to a signal magnitude value of 0. Using the boundaries for each water regime from the NUCLEUS program, i.e., clay-bound water: $T_2 < 3$ ms, bound (capillary) water: 3×10^{-3} s $< T_2 < 33 \times 10^{-3}$ s, and mobile water: 33×10^{-3} s $< T_2$, it can be seen that the saturated crushed marble stone and saturated round/quartz gravel had relaxation in every water regime. But, the saturated lawn quartz only had relaxation in the bound and mobile water regimes.

Figure 9 shows the pore-size distribution relating to signal magnitude for each fully saturated gravel-water mixture from borehole NMR. Each curve for each gravel sediment was the exact same shape as the T_2 curves in figure 8a, i.e., there was a linear relationship between pore size and transverse relaxation. Also, the signal magnitude for each curve in the pore-size distribution data and T_2 data was the exact same in figures 9 and 8a. The only difference was that the pore sizes are at a smaller magnitude than the transverse relaxation times. The range of pore sizes for crushed marble stone is $\approx 10^{-7}$-10^{-3} m, for round/quartz gravel the range is $\approx 10^{-8}$-10^{-4} m, and for lawn quartz the range of pore sizes is 10^{-6}-10^{-3} m.

Figure 10 shows the T_2 curves relating to signal magnitude for each fully saturated gravel-water mixture from the rock analyzer. It can be seen from this figure that each gravel sediment exhibited relaxation at higher T_2 values. The range of relaxation for each gravel sediment was the same, in the range of $\approx 10^{-1}$-10^{1} s. The relationship between transverse relaxation time and signal magnitude from figure 10 is that, the greater the T_2 at the peak of the curve, the smaller the value of the signal magnitude corresponding to this peak. Also, the signal magnitude was very high compared to the T_2 curves in figure 8a. Comparing the rock analyzer and borehole NMR T_2 data sets, figure 10 only shows one 'big' curve for each gravel sediment, where as the T_2 spectra in figure 8a have multiple curves for each gravel sediment.

4.1.2   Sand
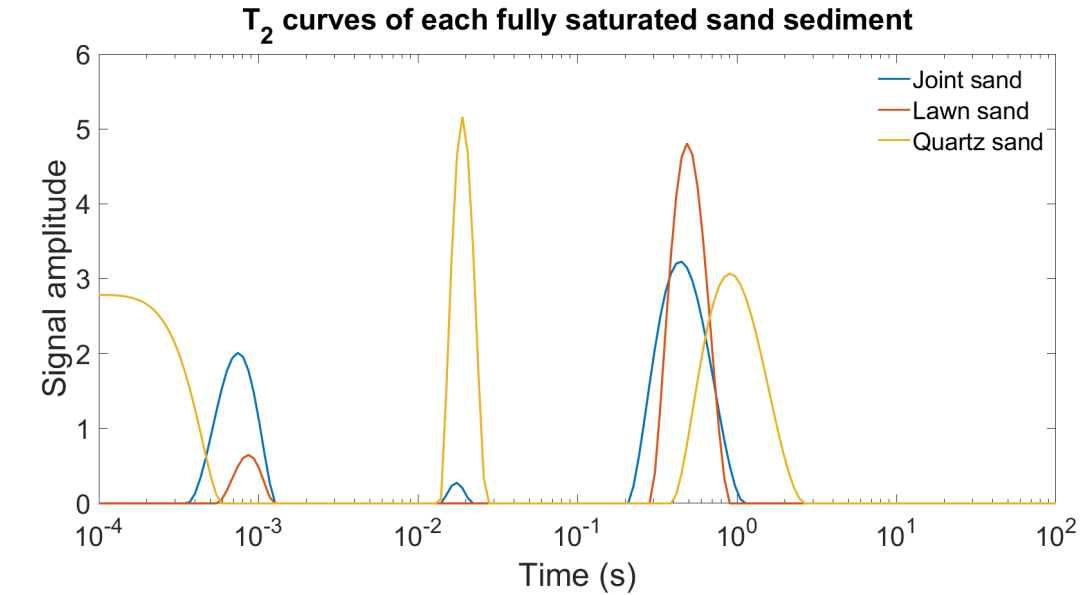
(a) T_2 relaxation times from three borehole NMR experiments using fully saturated sand-water mixtures.

(b) Spin echo decay curves in three fully saturated sand-water mixtures.

Figure 11: Graphs showing the T_2 relaxation and decay curves of fully saturated sand-water mixtures with data obtained from borehole NMR experiments. The exact degree of saturation for each sediment can be found in appendix A.1.
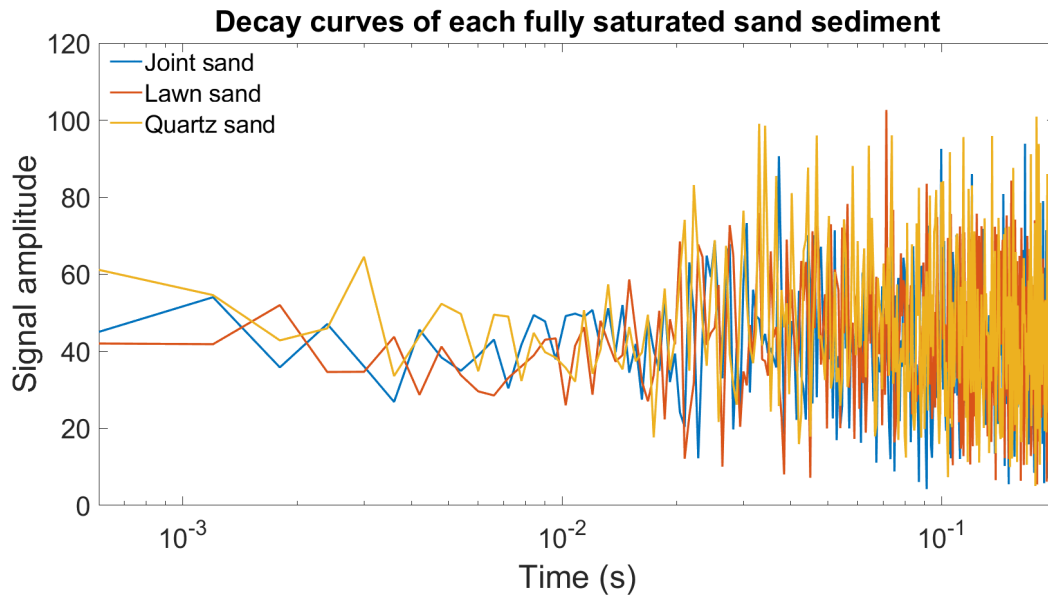
Figure 11 shows the T_2 and decay curves relating to signal magnitude for each saturated gravel-water mixture from borehole NMR. It can be seen that all of the sand sediments exhibited relaxation at high and low T_2 values except lawn sand which does not show any relaxation at 'middle' T_2 values. All of the sand sediments even showed relaxation at similar T_2 values, for example around $T_2 = 10^{-3}$ seconds both joint and lawn sand show relaxation and in the range of 10^{-1}-10^1 seconds, all three sand sediments exhibit relaxation. Using the boundaries for each water regime from the NUCLEUS

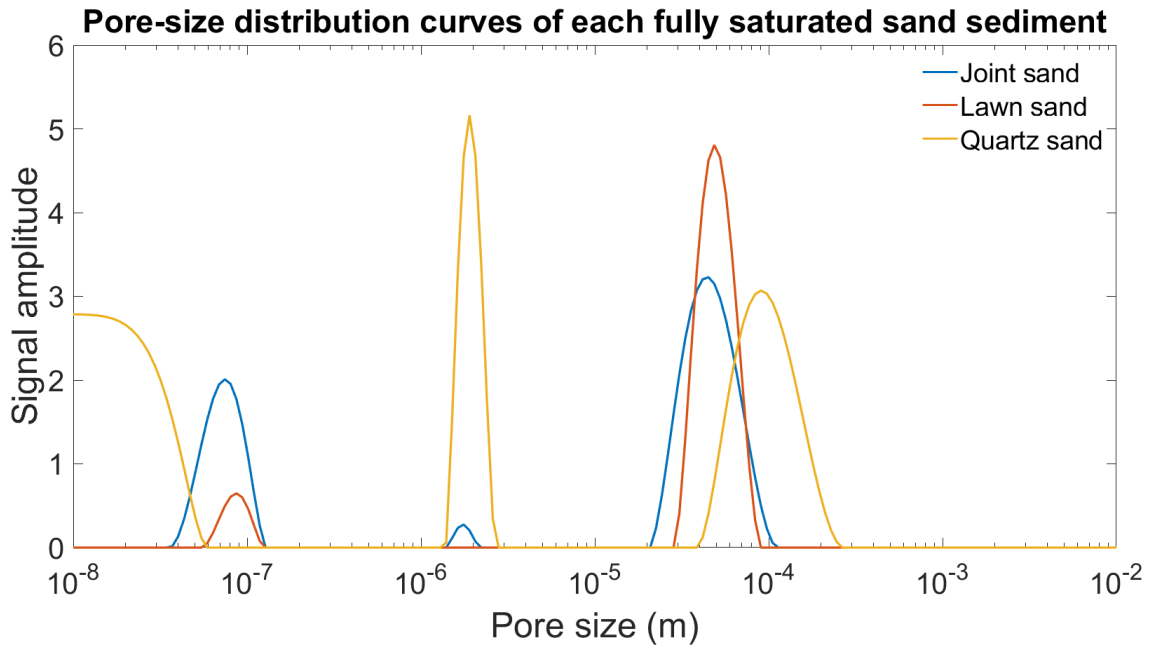Figure 12: Pore-size distribution curves of fully saturated sand-water mixtures with data obtained from borehole NMR experiments. The exact degree of saturation for each sediment can be found in appendix A.1.
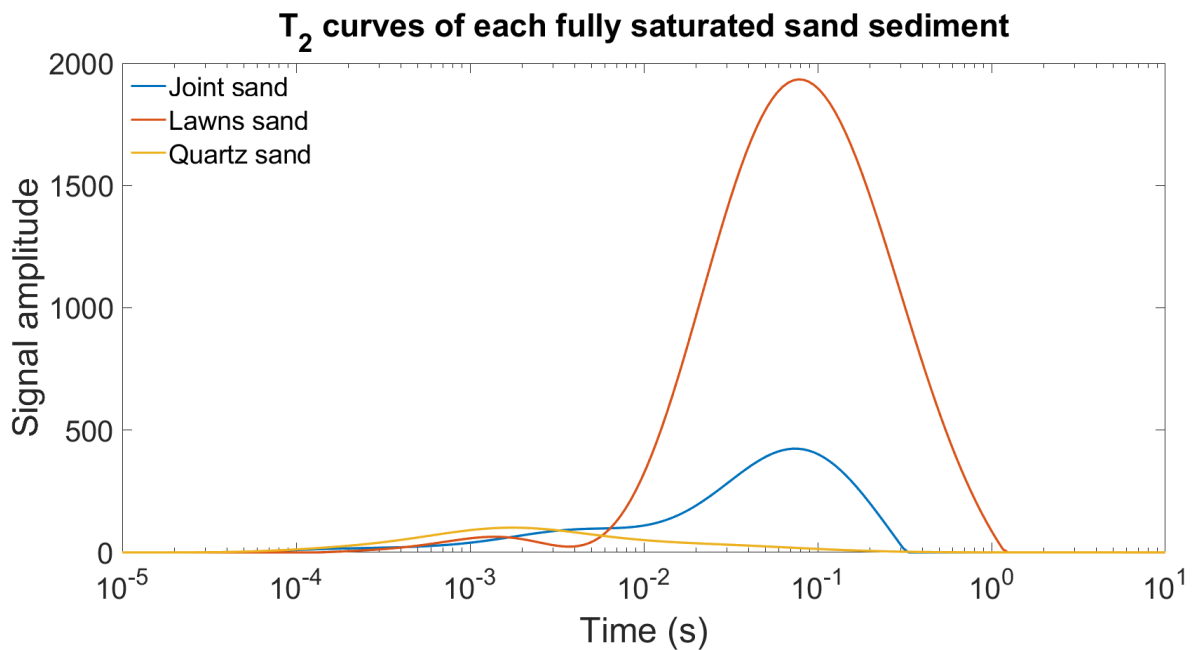

Figure 13: T_2 relaxation curves of fully saturated sand-water mixtures with data obtained from rock analyzer experiments. The exact degree of saturation for each sediment can be found in appendix B.1.

program, i.e., clay-bound water: $T_2 < 3$ ms, bound (capillary) water: 3×10^{-3} s $< T_2 < 33 \times 10^{-3}$ s, and mobile water: 33×10^{-3} s $< T_2$, it can be seen that the saturated joint sand and quartz sand had relaxation in every water regime. But, the saturated lawn sand only had relaxation in the clay-bound and mobile water regimes. An interesting observation from figure 11a was that for quartz sand, there was a decrease in signal amplitude in the clay-bound water regime and this did not occur for the other sand sediments. This could be an anomaly since this was not a common feature of T_2 spectra. Except from this initial decrease in signal magnitude, it can be seen in figure 11a that every curve for each sand sediment was separate, and not joined with another i.e., each curve increases from a signal magnitude of 0, reaches a peak value, and then decreases back to a signal magnitude value of 0

Figure 12 shows the pore-size distribution relating to signal magnitude for each fully saturated sand-water mixture from borehole NMR. Each curve for each sand sediment was the exact same shape as the T_2 curves in figure 11a, i.e., there was a linear relationship between pore size and transverse relaxation. Also, the signal magnitude for each curve in the pore-size distribution data and T_2 data was the exact same in figures 12 and 11a. The only difference was that the pore sizes are at a smaller magnitudes than the transverse relaxation times. The range of pore sizes for joint sand is $\approx 10^{-7}$-10^{-4} m, for lawn sand the range is $\approx 10^{-7}$-10^{-4} m, and for quartz sand the range of pore sizes is 10^{-8}-10^{-4} m. Except for the pore size of just above 10^{-6} m, all the sand sediments exhibit a change in signal magnitude at the same pore sizes which suggests the pore structure of these sands was similar despite their particle size varying.

Figure 13 shows the T_2 curves relating to signal magnitude for each fully saturated sand-water mixture from the rock analyzer. It can be seen from this figure that each sand sediment exhibited relaxation at high T_2 values. The range of relaxation for joint and lawn sand was the same, in the range of $\approx$ 10^{-2}-10^{0} s, but quartz sand was the only sand sediment which didn't show significant relaxation, i.e., the signal magnitude was very small compared to that of joint and lawn sand. Also, the signal magnitude of the T_2 spectra in figure 13 was very high compared to the T_2 spectra in figure 11a. Figure 13 only shows one 'big' curve for each sand sediment, where as the T_2 spectra in figure 11a had multiple curves for each sand sediment.

4.2   Saturation level $S_r \approx 0.500$

4.2.1   Gravel
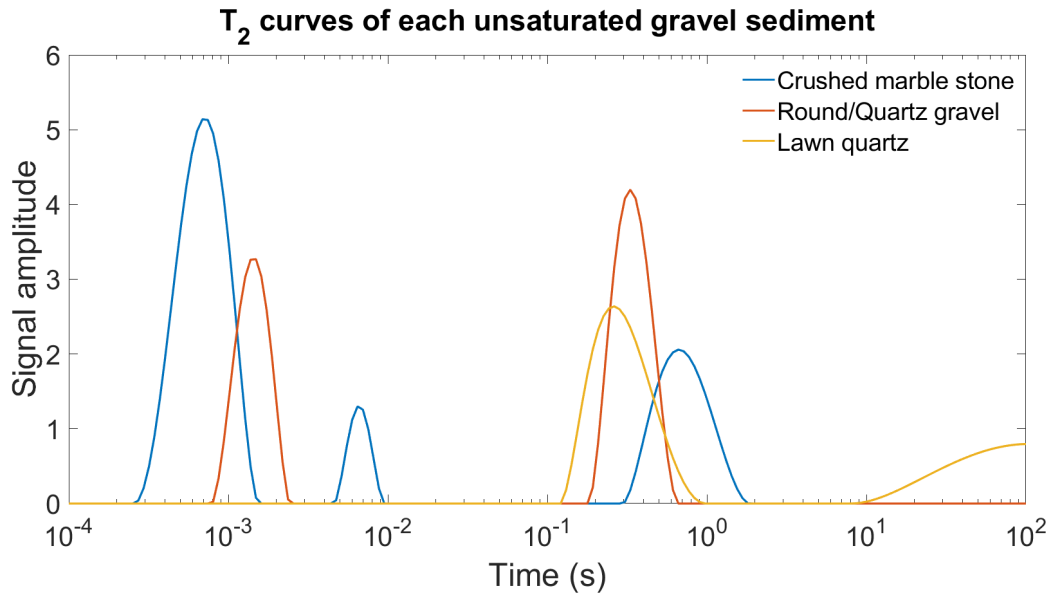
(a) T_2 relaxation times from three borehole NMR experiments using unsaturated gravel-water mixtures.
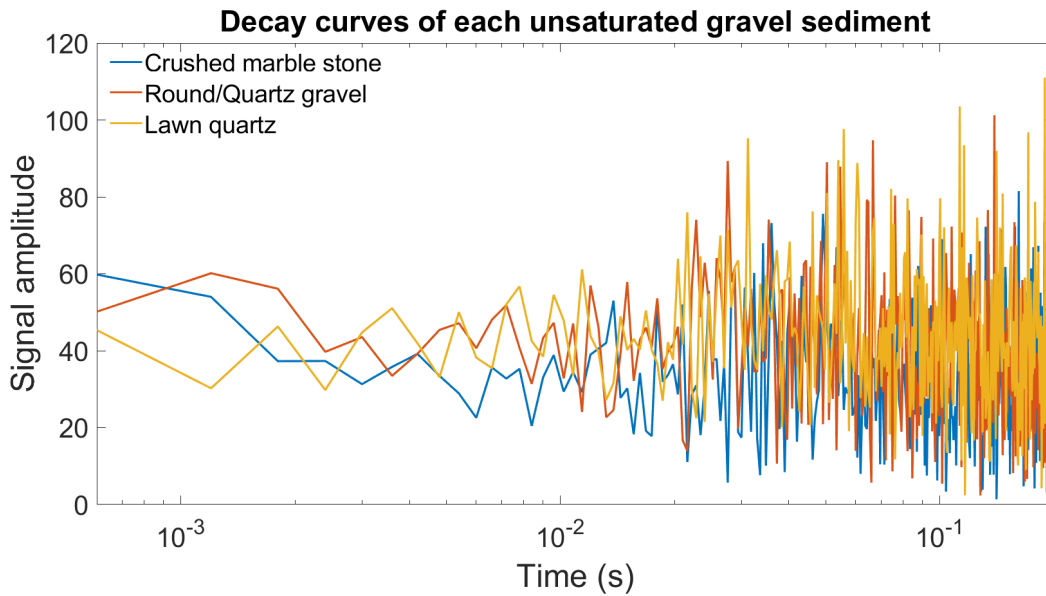
(b) Spin echo decay curves in three unsaturated gravel-water mixtures.

Figure 14: Graphs showing the T_2 relaxation and decay curves of unsaturated gravel-water mixtures with data obtained from borehole NMR experiments. The exact degree of saturation for each sediment can be found in appendix A.2.

Figure 14 shows the T_2 and decay curves relating to signal magnitude for each unsaturated gravel-water mixture from borehole NMR ($S_r \approx 0.500$). Lawn quartz was the only gravel sediment at this saturation level which had one relaxation curve on its spectra compared to the other two gravel sediments, and this was the same pattern observed from the T_2 spectra of the fully saturated gravel-water mixtures in figure 8a. It can also be seen in figure 14a that every curve for each unsaturated gravel
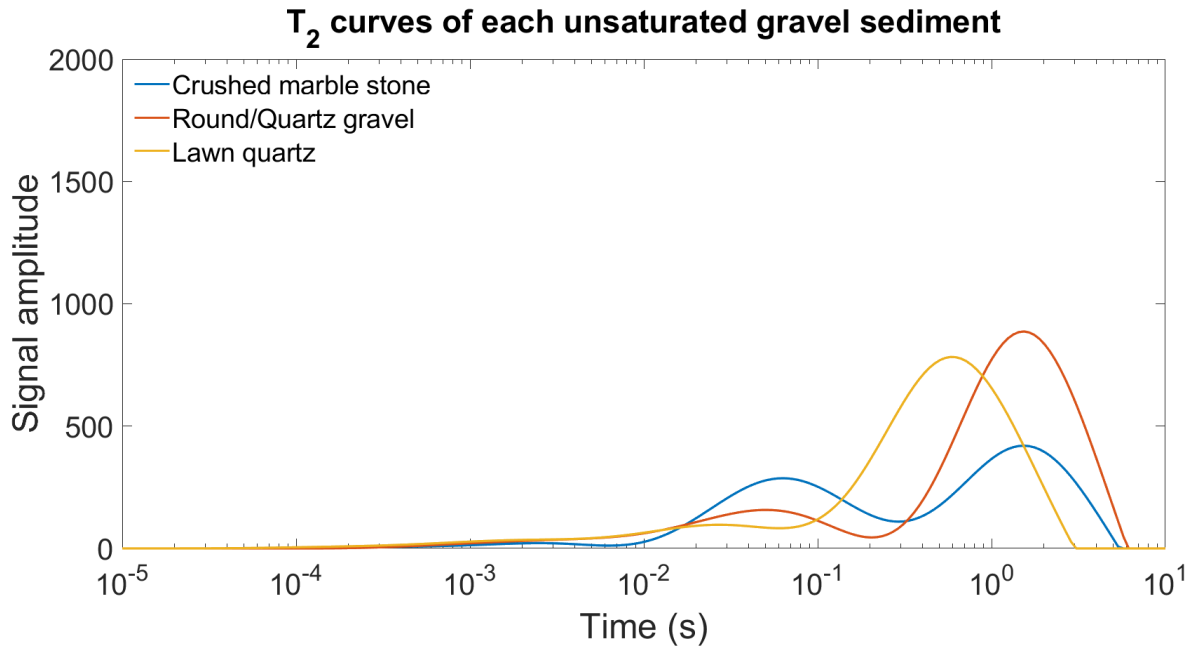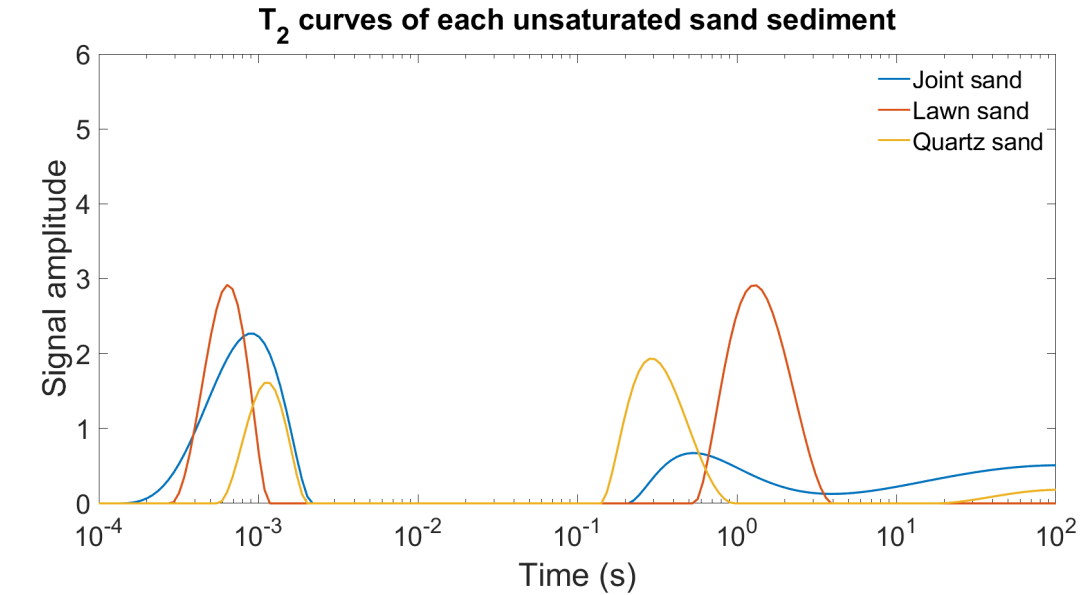
Figure 15: T_2 relaxation curves of unsaturated gravel-water mixtures with data obtained from rock analyzer experiments. The exact degree of saturation for each sediment can be found in appendix B.2.

sediment was separate, and not joined with another i.e., each curve increases from a signal magnitude of 0, reaches a peak value, and then decreases back to a signal magnitude value of 0. However, from a T_2 value of 10^1 seconds the signal magnitude of the lawn quartz continuously increases which is unusual. Using the boundaries for each water regime from the NUCLEUS program, i.e., clay-bound water: $T_2 < 3$ ms, bound (capillary) water: 3×10^{-3} s $< T_2 < 33 \times 10^{-3}$ s, and mobile water: 33×10^{-3} s $< T_2$, it can be seen that unsaturated crushed marble stone had relaxation in every water regime. unsaturated round/quartz gravel had relaxation in the clay-bound and mobile water regimes, but unsaturated lawn quartz only had relaxation in the mobile water regime.

Figure 15 shows the T_2 curves relating to signal magnitude for each unsaturated gravel-water mixture, saturated to a degree of $S_r \approx 0.500$ from the rock analyzer. It can be seen from this figure that each gravel sediment exhibited relaxation as the T_2 value increases from 10^{-2} s. Also, the signal magnitude is very high compared to the T_2 curves in figure 14a. Figure 15 shows multiple curves for each unsaturated gravel sediment which are joint together i.e., the signal magnitude does not go back down to 0 and increases again before the peak of the next curve, where as the T_2 spectra in figure 14a had multiple separate curves for each fully saturated gravel sediment. The range of $T_2 = 10^{-1}\text{-}10^1$ s was where the peaks of the curves are for each unsaturated gravel sediment.

4.2.2   Sand

(a) T_2 relaxation times from three borehole NMR experiments using unsaturated sand-water mixtures.
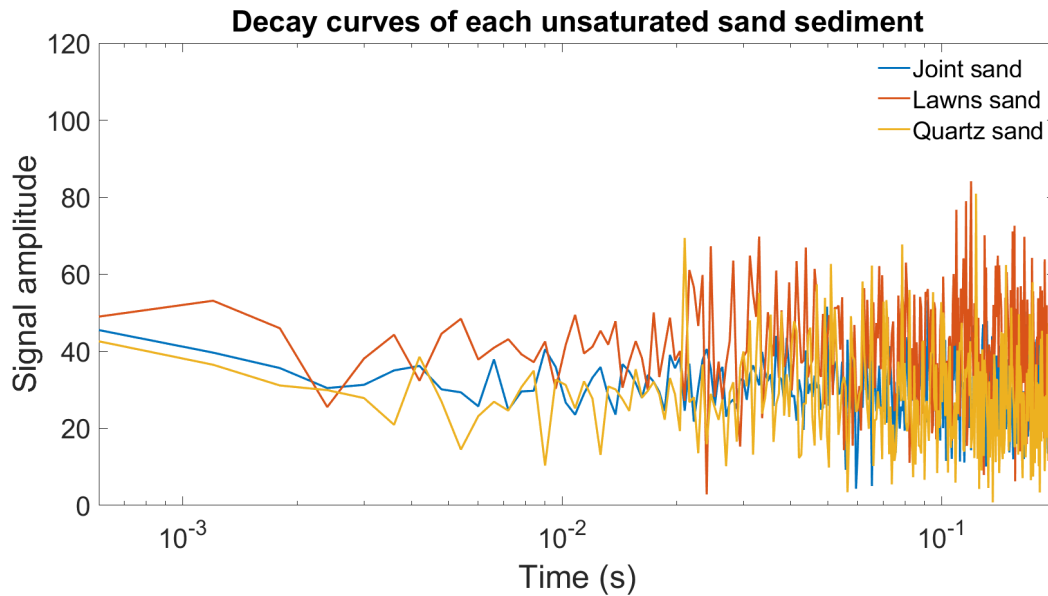
(b) Spin echo decay curves in three unsaturated sand-water mixtures.

Figure 16: Graphs showing the T_2 relaxation and decay curves of unsaturated sand-water mixtures with data obtained from borehole NMR experiments. The exact degree of saturation for each sediment can be found in appendix A.2.

Figure 16 shows the T_2 and decay curves relating to signal magnitude for each unsaturated sand-water mixture from borehole NMR ($S_r \approx 0.500$). It can be seen from this figure that each unsaturated sand sediment had two curves. The first set of relaxation curves occur around $T_2 = 10^{-3}$ s, with lawns and having the greatest signal magnitude out of the three. The next set of relaxation curves occur in a range of 10^{-1}-10^1 seconds, again with lawn sand having the greatest signal magnitude. Using the boundaries for each water regime from the NUCLEUS program, i.e., clay-bound water: $T_2 < 3$ ms,

Figure 17: T_2 relaxation curves of unsaturated sand-water mixtures with data obtained from rock analyzer experiments. The exact degree of saturation for each sediment can be found in appendix B.2.

bound (capillary) water: 3×10^{-3} s $< T_2 < 33 \times 10^{-3}$ s, and mobile water: 33×10^{-3} s $< T_2$, it can be seen that all the types of sand had relaxation in the clay-bound and mobile water regime, but not in the bound water regime. An interesting observation from figure 16a was that from a value of $T_2 \approx 10^{-1}$ s for joint sand, the curve never reaches 0 and continuously increases as the value of T_2 increases. Also, for quartz sand there was a small increase in signal magnitude from a T_2 value of $\approx 10^1$ s.

Figure 17 shows the T_2 curves relating to signal magnitude for each unsaturated sand-water mixture, saturated to a degree of $S_r \approx 0.500$ from the rock analyzer. It can be seen that for joint sand, the signal magnitude increased from 10^{-4}-$10^{-0.5}$ seconds with a large area below the relaxation curve, hence, the range of relaxation time for the joint sand was broad. This was similar to lawn sand and quartz sand Also, the signal magnitude of the T_2 spectra in figure 17 was very high compared to the T_2 spectra in figure 16a. Figure 17 shows one curve for each unsaturated sand sediment, where as the T_2 spectra in figure 16a had multiple curves for each sand sediment, but these were separated, where as the relaxation curves for each unsaturated sand sediment in figure 17 were continuous and don't go back down to a magnitude of 0 for the signal magnitude before terminating.

4.3 Saturation level $S_r \approx 0.100$

4.3.1 Gravel

(a) T_2 relaxation times from three borehole NMR experiments using unsaturated gravel-water mixtures.

(b) Spin echo decay curves in three unsaturated gravel-water mixtures.

Figure 18: Graphs showing the T_2 relaxation and decay curves of unsaturated gravel-water mixtures with data obtained from borehole NMR experiments. The exact degree of saturation for each sediment can be found in appendix A.3.

Figure 18 shows the T_2 and decay curves relating to signal magnitude for each unsaturated gravel-water mixture from borehole NMR ($S_r \approx 0.100$). It can be seen from this figure that unsaturated crushed marble stone and round/quartz gravel only had one relaxation curve. Round/quartz gravel's curve was centered around a value of $T_2 \approx 10^0$ s, but the relaxation curve for the unsaturated crushed marble stone was not really a curve, it was a continuous increase in signal magnitude as the value
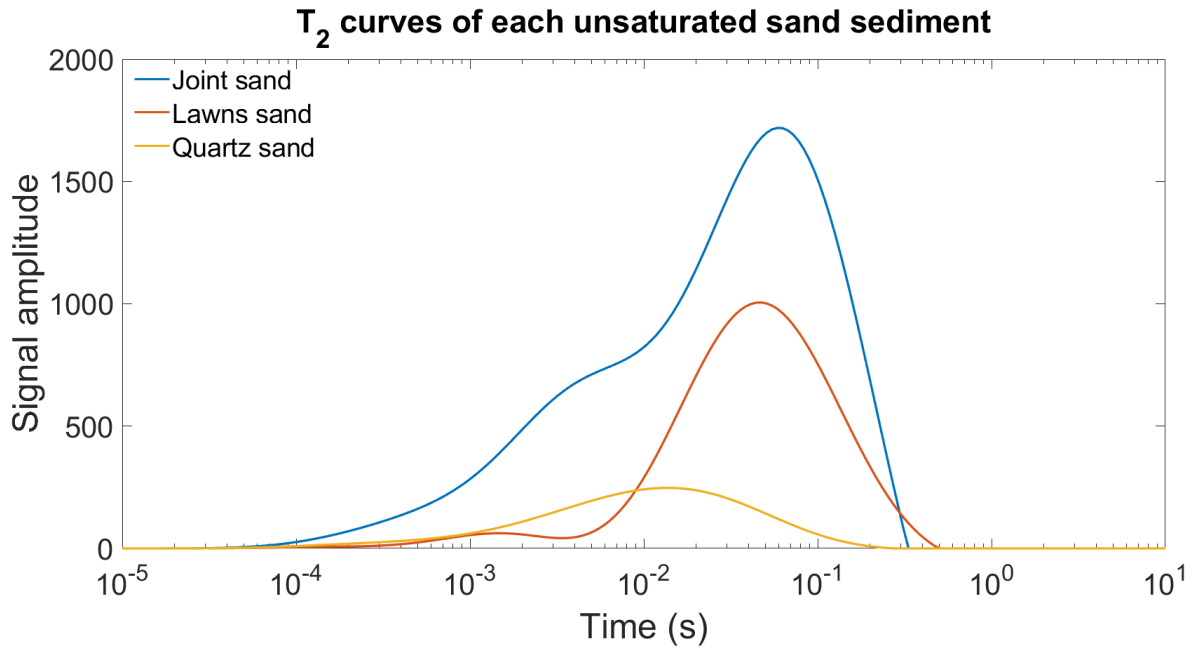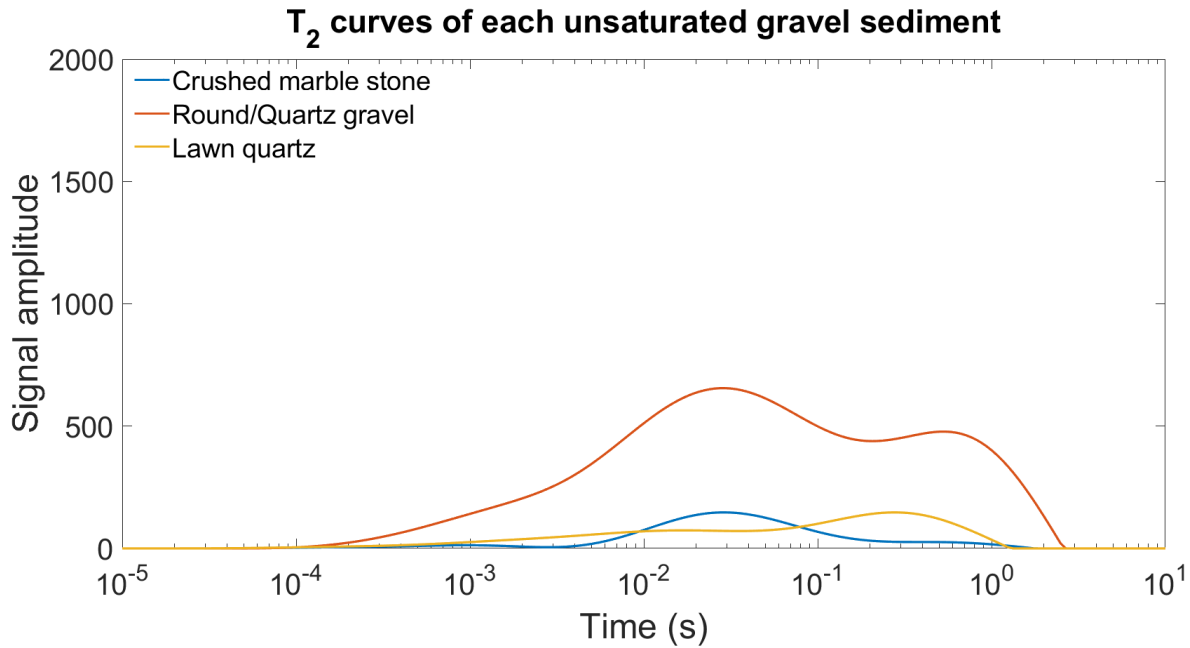
Figure 19: T_2 relaxation curves of unsaturated gravel-water mixtures with data obtained from rock analyzer experiments. The exact degree of saturation for each sediment can be found in appendix B.3.

of T_2 increased, this could be an anomaly since it wasn't observed on other crushed marble stone spectra. Lawn quartz has two curves which was the opposite trend compared to the other unsaturated and fully saturated gravel-water T_2 spectra in figures 14a and 8a. With one being in the almost exact same position as the relaxation curve of the unsaturated round/quartz gravel, and the other curve being much smaller, on the border of the clay-bound and bound water regimes. Using the boundaries for each water regime from the NUCLEUS program, i.e., clay-bound water: $T_2 < 3$ ms, bound (capillary) water: 3×10^{-3} s $< T_2 < 33 \times 10^{-3}$ s, and mobile water: 33×10^{-3} s $< T_2$, it can be seen that unsaturated crushed marble stone and round/quartz gravel only had relaxation in the mobile water regime, and unsaturated lawn quartz showed relaxation in the bound and mobile water regimes.

Figure 19 shows the T_2 curves relating to signal magnitude for each unsaturated gravel-water mixture, saturated to a degree of $S_r \approx 0.100$ from the rock analyzer. It can be seen from this figure that the curve for unsaturated round/quartz gravel had the broadest range out of the gravel sediments at this saturation level. The curve for unsaturated lawn quartz was also very spread out but the signal magnitude is much smaller compared to the signal magnitude of round/quartz gravel. Also, the signal magnitude in figure 19 was higher compared to the T_2 curves in figure 18a. An interesting observation from figure 19 is that the curves were not similar shapes compared to other T_2 spectra from the rock analyzer. Except for the unsaturated sand T_2 spectra below in figure 21, and the only similarity between these spectra was the degree of saturation. All the other T_2 spectra from the rock analyzer were from fully saturated or a higher degree of unsaturated sediment-water mixtures, and this could be a reason for the shapes of these spectra.

4.3.2   Sand

(a) The decay curves of protons in three unsaturated sand-water mixtures. Each curve is inverted to produce the data in fig
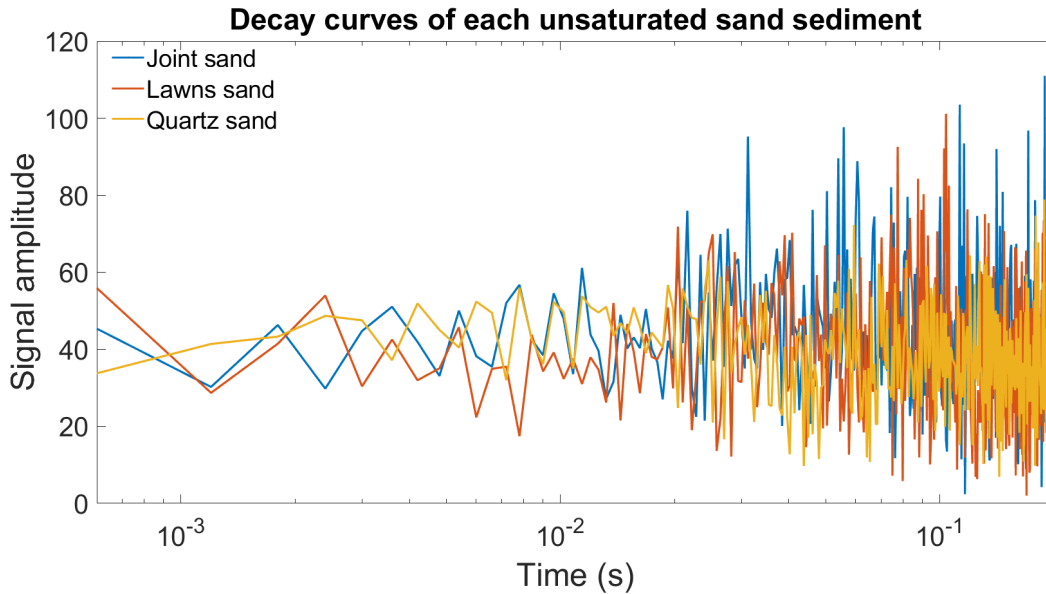
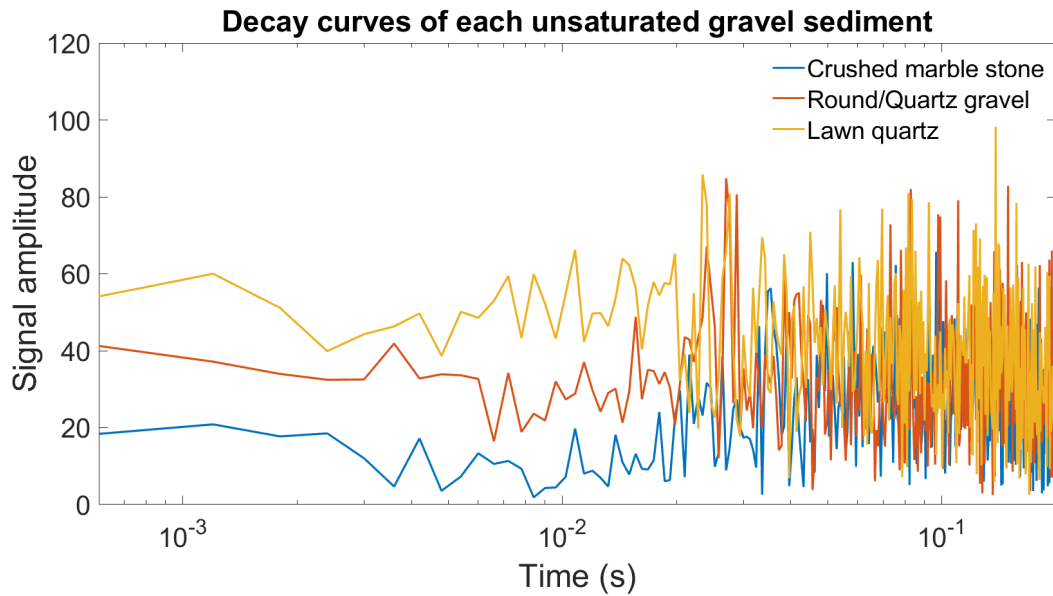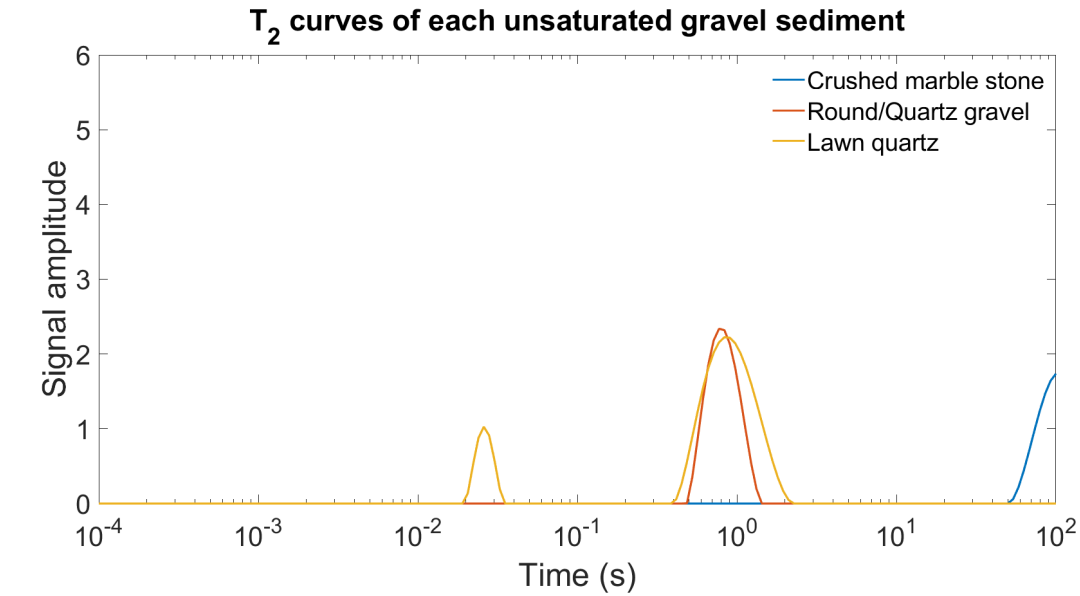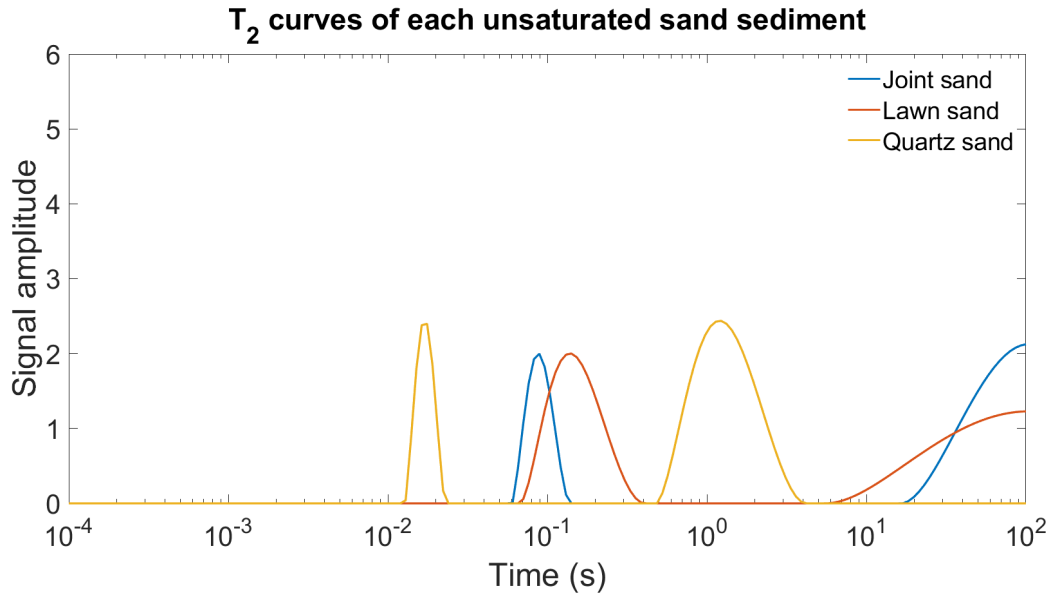(b) Spin echo decay curves in three unsaturated gravel-water mixtures.

Figure 20: Graphs showing the T_2 relaxation and decay curves of unsaturated sand-water mixtures with data obtained from borehole NMR experiments. The exact degree of saturation for each sediment can be found in appendix A.3.

Figure 20 shows the T_2 and decay curves relating to signal magnitude for each unsaturated sand-water mixture from borehole NMR ($S_r \approx 0.100$). Using the boundaries for each water regime from the NUCLEUS program, i.e., clay-bound water: $T_2 < 3$ ms, bound (capillary) water: 3×10^{-3} s $< T_2 < 33 \times 10^{-3}$ s, and mobile water: 33×10^{-3} s $< T_2$, it can be seen that unsaturated joint sand had relaxation in the bound and mobile water regimes, and, unsaturated lawn and quartz sand had relaxation in only the mobile water regime. Also, there was a range of T_2 values for all the curves
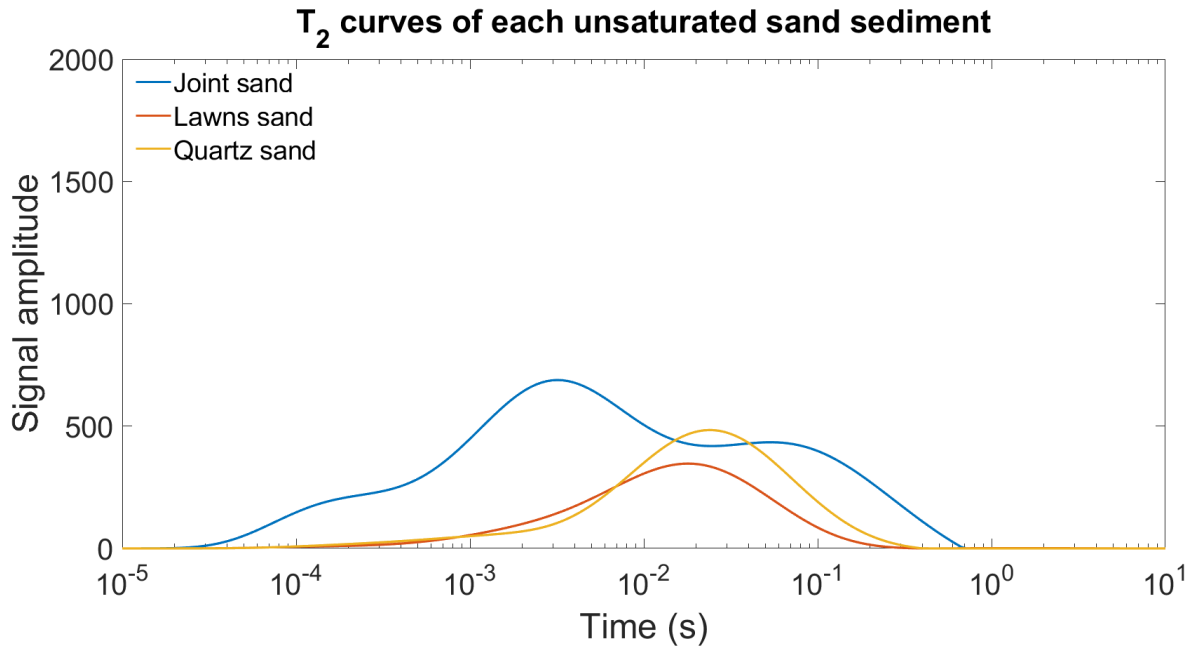
Figure 21: T_2 relaxation curves of unsaturated sand-water mixtures with data obtained from rock analyzer experiments. The exact degree of saturation for each sediment can be found in appendix B.3.

in figure 20a, for example, the curves occured in a range of $T_2 = 10^{-2}$-10^1 s. The only similar value for the curves was around $T_2 = 10^{-1}$ s, and these are the first curves of unsaturated joint and lawn sand. An interesting observation that can be seen in figure 20a was the increase in signal magnitude for the relaxation curves of unsaturated joint sand and lawn sand, as the value of T_2 increased from $\approx 10^1$ s. This was observed in other T_2 spectra for gravel and sand sediments, and these patterns could potentially be anomalies.

Figure 21 shows the T_2 curves relating to signal magnitude for each unsaturated sand-water mixture, saturated to a degree of $S_r \approx 0.100$ from the rock analyzer. It can be seen from this figure that within the range of $T_2 = 10^{-4}$-10^0 s, there was relaxation for all the unsaturated sand sediments. The T_2 curve of joint sand has the broadest range and highest signal magnitude. Also, the peak of the curves for lawn sand and quartz sand occur at a similar value around $T_2 = 10^{-2.5}$ s. Figure 21 showed one curve for each unsaturated sand sediment, where as the T_2 spectra in figure 20a had multiple curves for each sand sediment, but these were separated, where as the relaxation curves for each unsaturated sand sediment in figure 21 were continuous and don't go back down to a magnitude of 0 for the signal magnitude before terminating. An interesting observation from figure 21 was that the curves are not similar shapes compared to other T_2 spectra from the rock analyzer. Except for the unsaturated sand T_2 spectra above in figure 19, and as mentioned before, the only similarity between these spectra was the degree of saturation. All the other T_2 spectra from the rock analyzer were from saturated or a 'higher degree' of unsaturated sediment-water mixtures, and this could be a reason for the shapes of these spectra.
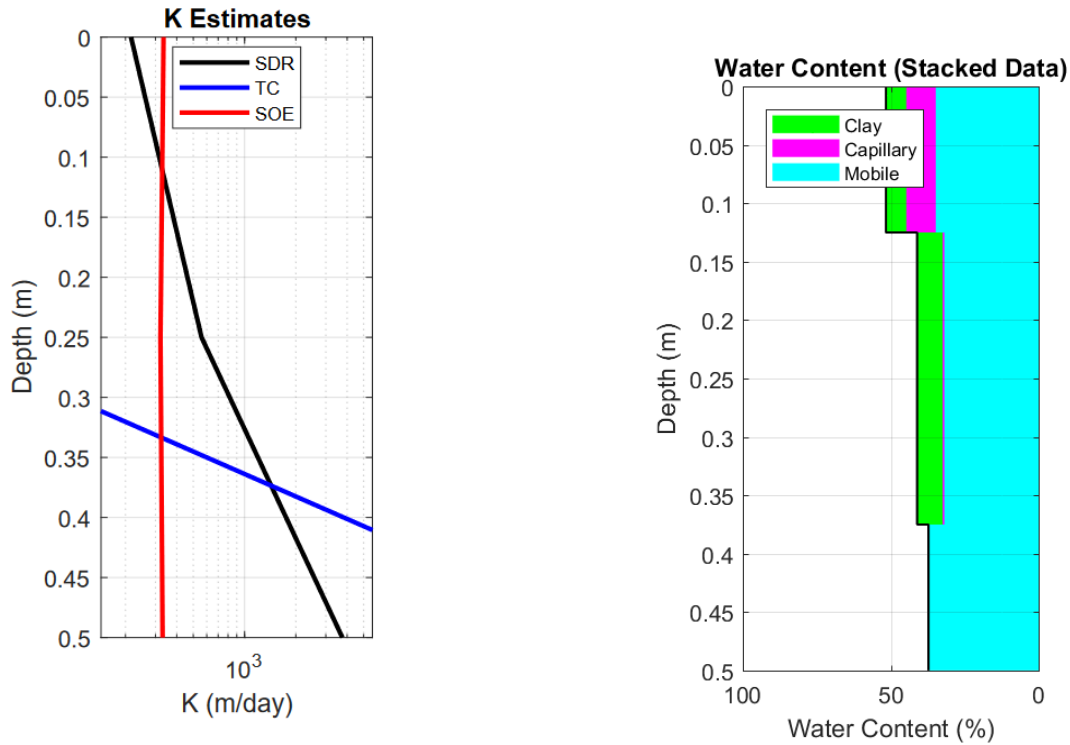
(a) Estimates of hydraulic conductivity of fully water saturated crushed marble stone.

(b) Estimates of water content of fully water saturated crushed marble stone.

Figure 22: Data sets obtained from the DART probe showing estimates of hydraulic conductivity, and water content with depth of the borehole from an experiment using a fully saturated crushed marble stone-water mixture.

4.4   Hydraulic conductivity and water content estimates from borehole NMR

Shown in subsection 4.4 is data regarding estimates of hydraulic conductivity (K) and water content from borehole NMR of each experiment using a saturated sediment-water mixture. This section only contains data from the fully saturated sediment-water mixtures because these are the valid estimates. The water content is obtained from the amplitude of NMR curves which relate to the relaxation time. It can be seen in every data set for the hydraulic conductivity, for the estimate of K there are three equations. Namely, Schlumberger-Doll research equation (SDR), Timur-Coates (TC) and sum of echoes (SOE). I have focused on the SOE equation since this relatively stays the same with the depth of the borehole for all the fully saturated sediment-water mixtures.

Figure 22 shows the estimates of hydraulic conductivity (K) and water content from the DART probe from the saturated crushed marble stone sample. It can be seen that both the K and water content estimates varied with depth. It can be seen that the estimate of K from the SOE equation varied little with depth. Specifically, from about halfway in the borehole from 0.25 m towards the deeper depths, the SOE estimate of K basically was constant with a value between 10^2-10^3 m/day. Figure 22b shows how the water content varies with depth of the borehole. It can be seen in this figure there was clay, capillary and mobile water present in this fully saturated crushed marble sample. It can be seen that at all depths mobile water was present and it relatively stayed the same throughout the pipe. Both clay and capillary water are present in the pipe but only up until a depth of about 0.37 m.

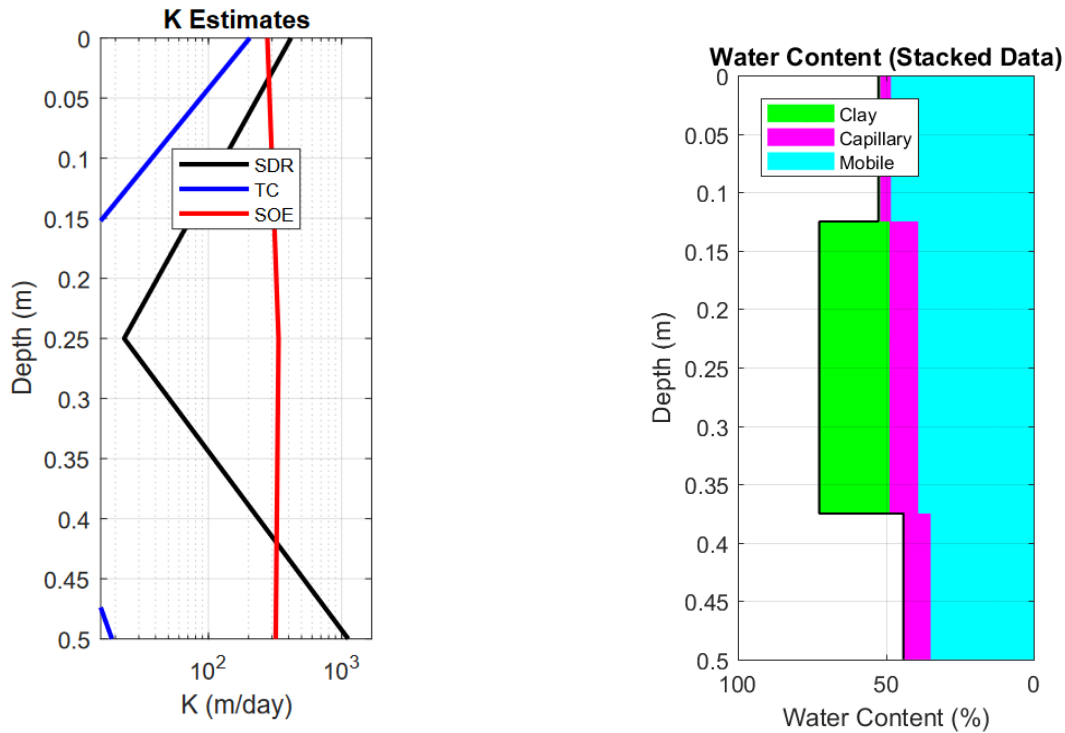(a) Estimates of hydraulic conductivity of fully water saturated round/quartz gravel.

(b) Estimates of water content of fully water saturated round/quartz gravel.

Figure 23: Data sets obtained from the DART probe showing estimates of hydraulic conductivity, and water content with depth of the borehole from an experiment using a fully saturated round/quartz gravel-water mixture.

Another interesting observation that can be seen from figure 22b about these 2 water regimes is that at the shallow depths of 0.00-0.12 m, there was a higher % of capillary than clay water but then at the depths of 0.12-0.37 m, there was more clay than capillary water. So, for this fully saturated crushed marble sample, the depth of 0.12 m was a turning point for the switching of the clay and capillary water regimes in terms of which one has a greater % present. The clay and capillary water presence in figure 22b ceased to exist at the lowest depths of the pipe. Nevertheless, throughout the crushed marble in the borehole, mobile water had the biggest presence.

Figure 23 shows the estimates of hydraulic conductivity (K) and water content from the DART probe from the saturated round/quartz gravel sample. It can be seen that the SOE estimate of K in figure 23a was a similar value of K compared to figure 22a. This implies that for fully water saturated gravel mixtures, the value of K is the same no matter what type of gravel if one focuses on the SOE estimate, i.e., K was a value between 10^2-10^3 m/day. Figure 23b shows how the water content varies with depth of the borehole. It can be seen there was clay, capillary and mobile water present in this fully saturated round/quartz gravel sample. It can be seen from this figure that the % of mobile water slightly reduced as the depth increased and in the middle of the type all 3 types of water regimes were present. Mobile and capillary water were present throughout the round/quartz gravel in the borehole where as there was only clay water in this round/quartz gravel sample in the mid-depth region of the borehole. This big bulk of clay water in the mid-depths of the round/quartz gravel in the borehole was similar to the data shown in figure 22b, in the sense there was more clay water in gravel/water
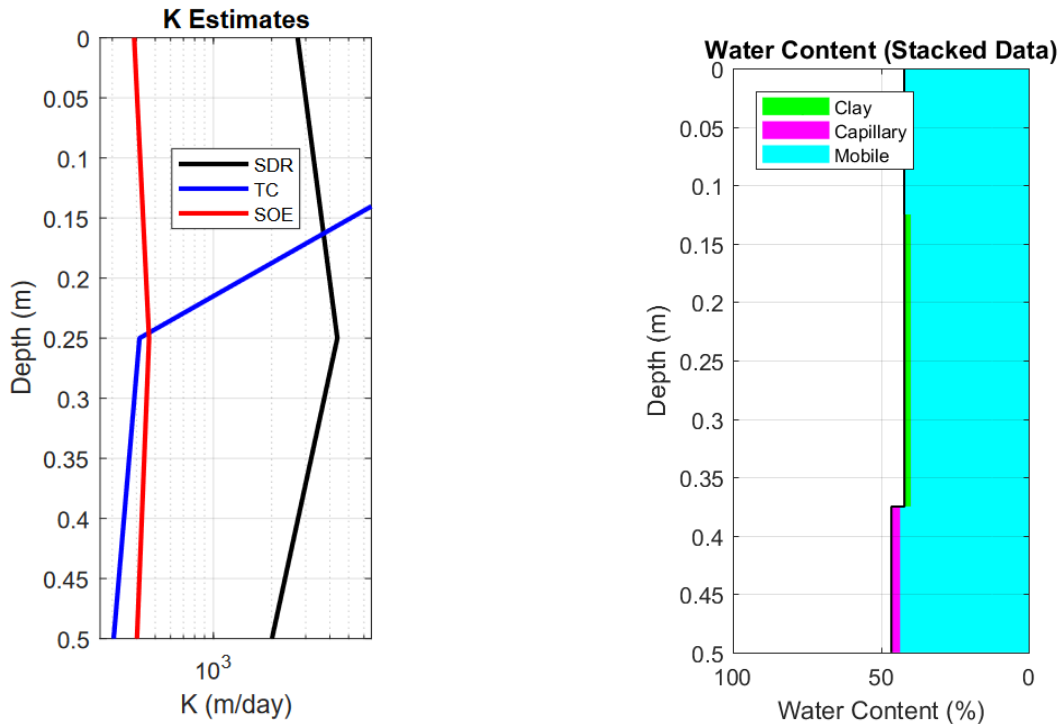
(a) Estimates of hydraulic conductivity of fully water saturated lawn quartz.

(b) Estimates of water content of fully water saturated lawn quartz.

Figure 24: Data sets obtained from the DART probe showing estimates of hydraulic conductivity, and water content with depth of the borehole from an experiment using a fully saturated lawn quartz-water mixture.

mixture in the mid-depths of the borehole compared to other regions.

Figure 24 shows the estimates of hydraulic conductivity (K) and water content from the DART probe from the saturated lawn quartz sample. It can be seen in figure 24a that at around a depth of 0.25 m the relationship between K and depth of the borehole changed for all estimates of K, it switched from increasing to decreasing. This being said, the value of K was roughly the same as the value of K from the other fully saturated gravel-water experiments, as can been by comparing the data shown in figure 24a to figures 22a and 23a. The SDR and SOE estimates of K showed a similar pattern, but the SDR estimate of K was at a larger magnitude than the SOE estimate. This being said, for the depths of the borehole shown in figure 24a, K was a value between 10^2-10^3 m/day. Figure 24b shows how the water content varies with depth of the borehole. It can be seen in this figure that at all depths mobile water was present which is similar to the other fully saturated gravel-water experiments. There was only a small presence of clay and capillary water with neither type co-existing with the other, i.e., there was never any clay and capillary water together in this lawn quartz sample in the borehole.

Figure 25 shows the estimates of hydraulic conductivity (K) and water content from the DART probe from the saturated joint sand sample. It can be seen from the SOE estimate of K in figure 25a, at first, the value of K slightly decreased as the borehole depth increases, and then at a depth of 0.25 m the relationship changes. Even though this data is from joint sand, this value for K is similar to the K estimate from the fully water saturated gravel experiments which shows for saturated unconsolidated

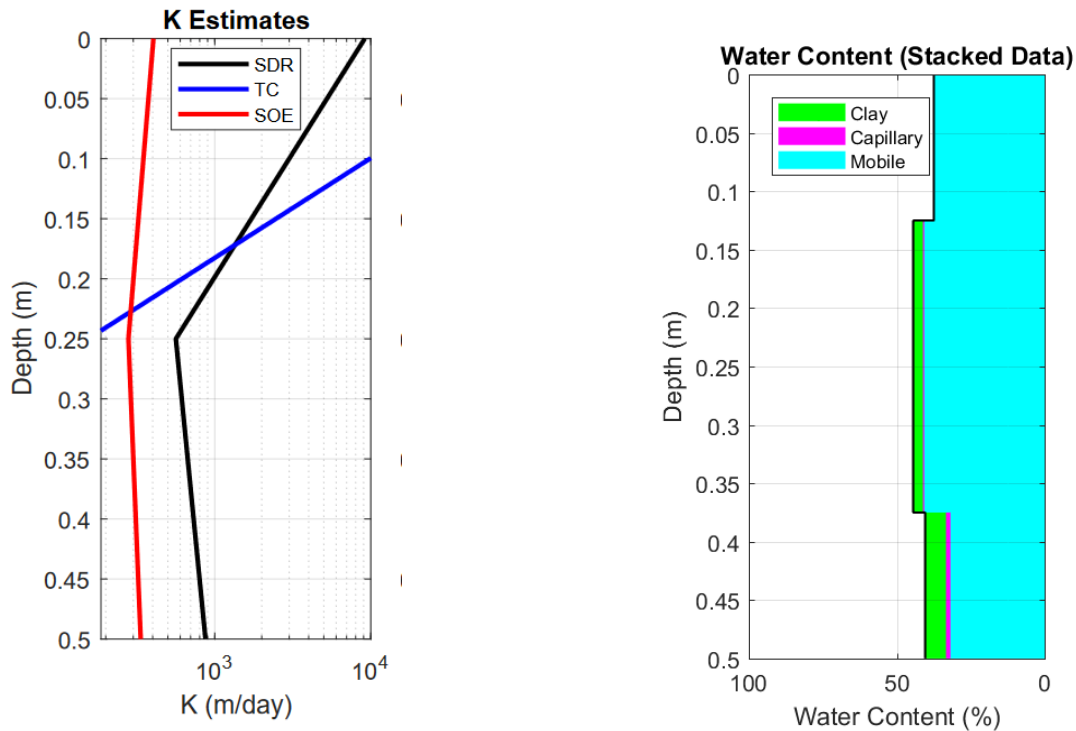(a) Estimates of hydraulic conductivity of fully water saturated joint sand.

(b) Estimates of water content of fully water saturated joint sand.

Figure 25: Data sets obtained from the DART probe showing estimates of hydraulic conductivity, and water content with depth of the borehole from an experiment using a fully saturated joint sand-water mixture.

sediment-water mixtures in a borehole, the value of K is about 10^2 - 10^3 m/day like with joint sand. Another interesting observation from figure 25a is the shape of the SOE estimate of K was 'reflected' in a mirror compared to the SOE estimate of K in figures 23a and 24a. Figure 25b shows how the water content varied with depth of the borehole. It can be seen there is clay, capillary and mobile water present in this saturated joint sand sample. It can be seen from this figure that mobile water had the greatest presence in this sample, being present at all depths. From a depth of about 0.13 m until the bottom of the pipe, there was the presence of clay water, although the quantity was a lot smaller than the amount of mobile water. Then, in the last 0.11 M or so of the pipe, there was a little amount of capillary water present.

Figure 26 shows the estimates of hydraulic conductivity (K) and water content from the DART probe from the saturated lawn sand sample. It can be seen from looking at the SOE estimate in figure 26a that the SOE estimate of K is almost constant. However, at a depth of 0.25 m in the pipe there was a little change in relationship of K with depth, and as the borehole depth increased, the value of K increases. This was similar to the fully saturated joint sand hydraulic conductivity data, as shown in figure 25a. Comparing figures 26a and 25a suggests that for fully saturated sand mixtures with water, the value of hydraulic conductivity remains practically the same with depth or it increases ever so slightly. The SOE and SDR estimates for K had a similar relationship with the depth of the pipe, the only difference being the SDR estimate was slightly larger value of K than the SOE estimate. Another interesting observation from figure 26a was the shape of the SOE estimate of K is 'reflected'

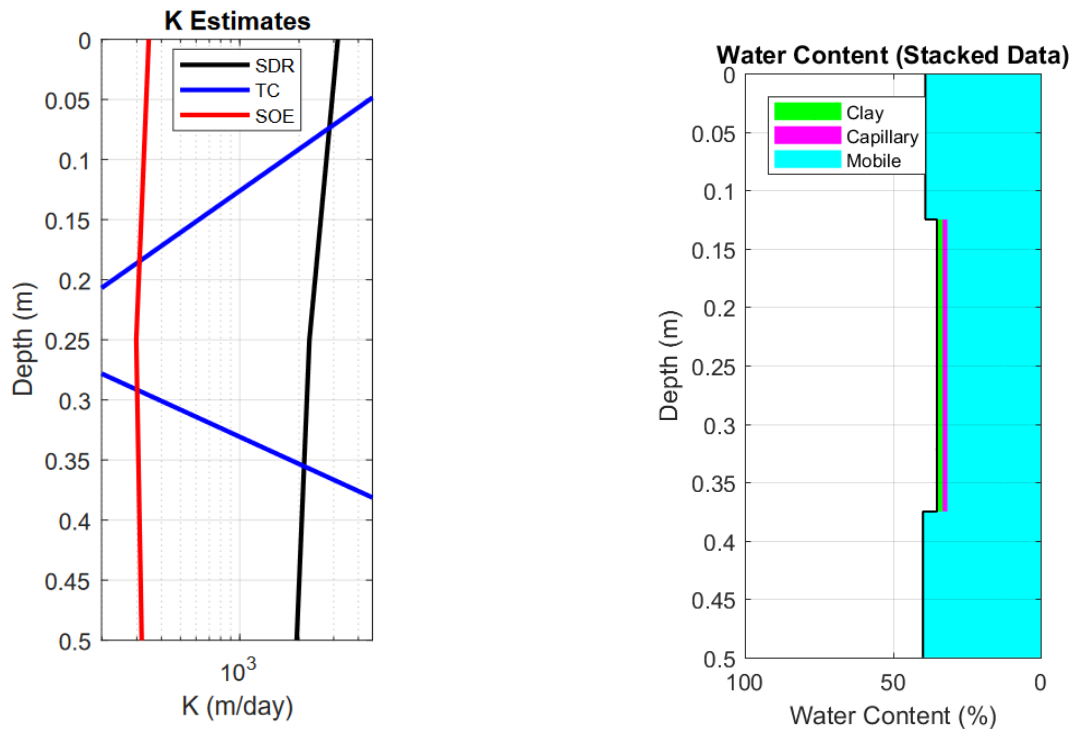(a) Estimates of hydraulic conductivity of fully water saturated lawn sand.

(b) Estimates of water content of fully water saturated lawn sand.

Figure 26: Data sets obtained from the DART probe showing estimates of hydraulic conductivity, and water content with depth of the borehole from an experiment using a fully saturated lawn sand-water mixture.

in a mirror, compared to the SOE estimate of K in figures 23a and 24a. Figures 26a and 25a showed the same trend for the SOE estimate of K which are both opposite to the trend of the SOE estimate of K in figures 23a and 24a. Figure 26b showed how the water content varies with depth of the borehole. It can be seen there is clay , capillary, and mobile water present in this fully saturated lawn sand sample, although the former two are only in a very small quantity. It can be seen that for the fully saturated lawn sand-water mixture there is a lot of mobile water, with slightly greater concentration at shallower & deeper depths. In the mid-depth region of the borehole where there was a tiny presence of clay and capillary water, the overall water content decreased.

Figure 27 shows the estimates of hydraulic conductivity (K) and water content from the DART probe from the saturated quartz sand sample. The SOE estimate of K in figure 27a was basically constant at all depths. Also, this value of K was similar to the other K values from the other fully saturated sand experiments which means no matter the type of sand, K is a very similar value according to the SOE estimate. In the latter 0.25 m of the borehole in figure 27a, the estimates of K from SOE and SDR were very similar which indicates for this fully water saturated quartz sand sample, a value for K between 10^2-10^3 m/day is highly probable. Figure 27b shows how the water content varies with depth of the borehole. It can be seen there was clay, capillary and mobile water present in this fully saturated quartz sand sample. Mobile water was the only regime present at all depths and it has the biggest concentration of the three. At the middle and lower depths of the quartz sand in the borehole there was more capillary water, although at the deeper depth the amount of capillary water is very

(a) Estimates of hydraulic conductivity of fully water saturated quartz sand.
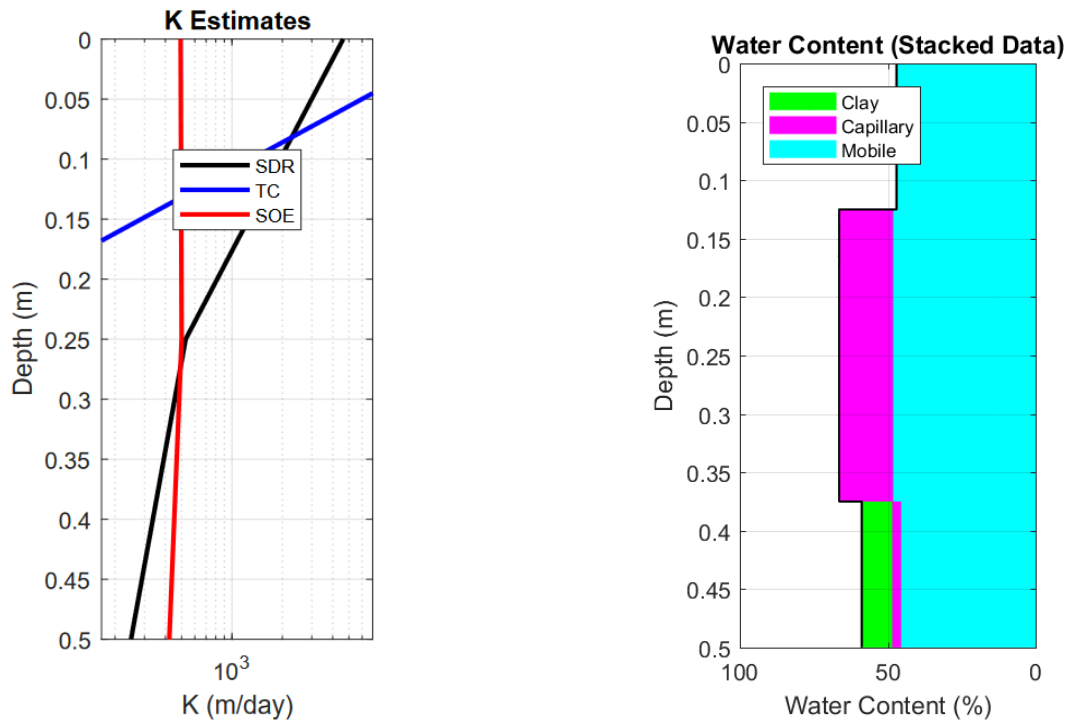
(b) Estimates of water content of fully water saturated quartz sand.

Figure 27: Data sets obtained from the DART probe showing estimates of hydraulic conductivity, and water content with depth of the borehole from an experiment using a fully saturated quartz sand-water mixture.

small. Then, in the latter 0.13 m of the borehole there there was clay water and this the only quartz sand in the borehole that had clay water. It seems for a fully saturated quartz sand-water mixture all three types of water regimes existed. Which is the same from all my experimental data regarding the saturated sand water content data set.

4.5   Derived water content from the rock analyzer

Shown in subsection 4.5 is self derived water content from each experiment performed using the rock analyzer using a sediment-water mixture. The data is displayed in a table for each sediment-water mixture at each saturation level. In order to calculate these values, linear regression analysis was used in the form of an equation of a linear line y = mx+c. For the rock analyzer there were 'standard samples' with known water contents, which had to be used to calibrate the rock analyzer before performing an experiment. In order to find the actual water content in the sample being measured, the known water content values of the 'standard samples' were used as an input for forming the equation of a line (x-axis). Each standard sample was placed into the core holder of the rock analyzer, and the 'MaxPeak' value from the signal values is used (y-axis), to form the equation of a linear line y = mx+c. Finally, the 'MaxPeak' value from each experiment I performed was used as the y-value in the equation of the linear line and the calculated x-value was the calculated water content in the sample. Therefore, it is essentially 'like a best fit'.

Table 1 below summarizes the calculated water content from each experiment using the rock analyzer. The units of the water content is in grams.

Saturation level S_r / Material	Crushed Marble	Round gravel	Lawn quartz	Joint sand	lawn sand	Quartz sand
≈ 0.100	1.485	3.714	2.116	2.791	3.825	1.316
≈ 0.500	5.416	7.705	6.954	6.614	9.289	3.972
≈ 1.000	8.070	8.444	14.075	4.196	20.541	5.013

It can be seen from table 3 above that the general trend was, as the degree of saturation increased, the mass of water in each sediment-water mixture also increased. Intuitively, this made sense because, roughly the dry mass of each sediment was the same in each experiment (range from 0.147-0.282 $\pm$ 0.0005 kg) and hence, there should be more water in the higher saturated sample because a higher degree of saturation means more water present. However, there were three considerable anomalies in table 3. Firstly, for joint sand, according to calculations, there was more water in the unsaturated sample ($S_r \approx 0.500$), compared to the saturated sample. The other two outliers are the calculated water content values in the saturated lawn quartz and lawn sand samples since these values were very high compared to all the other water content values at the same saturation level. However, all the values in table 3 seemed very high considering the calculated wet masses of the sediments used, were smaller than the values in table 3. It should be noted every experiment contained noise so this could be a factor for the results. Ignoring the high water content values in table 3 briefly, a difference with the lawn quartz water content data compared to the other gravel water content data in this table for crushed marble and round/quartz gravel, is that the amount of water in the saturated lawn quartz-water sample ($S_r \approx 1.000$) was significantly higher than than the amount of water in the saturated crushed marble and lawn quartz samples. This mass of 14.075 g in the saturated lawn quartz sample seemed very high. Also, for the saturated joint sand sample ($S_r \approx 1.000$) there was less water than the unsaturated joint sand sample ($S_r \approx 0.500$). This could be an anomaly since the dry masses of the joint sand at each saturation level were roughly the same. A difference with the lawn sand water content data compared to the other sand-water content data in this table is that the amount of water in the saturated lawn sand sample ($S_r \approx 1.000$) is significantly higher than than the amount of water in the saturated joint sand and quartz sand samples. This could be an anomaly since the dry masses of the joint sand at each saturation level were roughly the same.

5   Discussion

Before the discussion begins, some figures are presented which will be used as a comparison for some of my data. Firstly, an example of T_2 curves relating to pore size are shown in figure 28 which is taken from [9] and [13]. This figure shows the theoretical size of the pores based on the relaxation time T_2. This was one resource used to help interpret and discuss the T_2 and pore-size distribution spectra shown in this thesis.
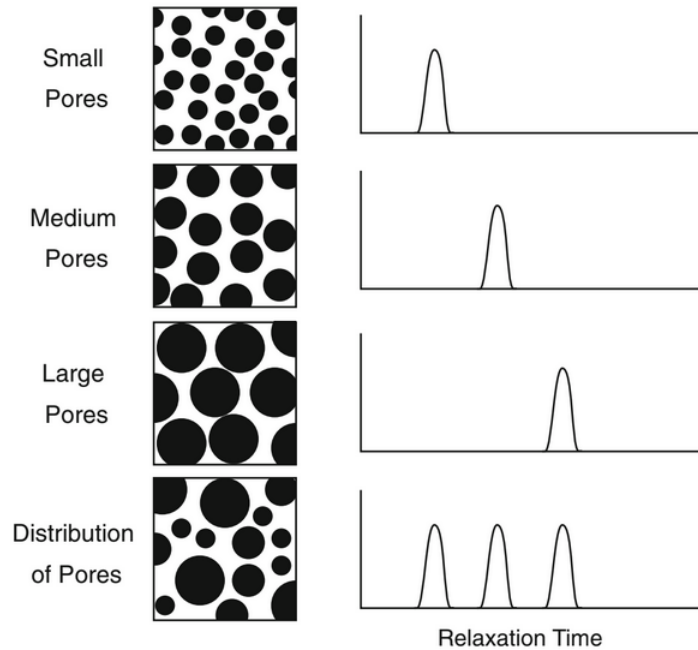
Figure 28: Graphs showing the possible pore size based on the relaxation time value T_2. Image from [9] and [13].

Secondly, figure 29 shows data from a research group in China [31] regarding the transverse relaxation time T_2 and pore-size distribution of a gravel-sand mixture.The data in figure 29 was used as a comparison for the transverse relaxation time T_2 and pore-size distribution data in this thesis, regarding the experimental borehole NMR data, and transverse relaxation time T_2 from the rock analyzer results regarding gravel. It should be noted that the sediment mixture used by Feng et al [31] to get the data shown in figure 29 had a ratio of 70/30 gravel/sand so this was one slight difference compared to the experiments in this thesis (I performed gravel and sand sediments separately). The set up used by Feng et al was fairly similar compared to the rock analyzer used in this thesis. Even though Feng et al [31] used lab NMR, their experimental method was a little different, for example they introduced 'suffusion' into their method so this could be a reason for difference in their T_2, and pore-size distribution data and mine. Also, the gravel-sand-water mixture used by Feng et al [31] was fully saturated, where as some of my data consists of unsaturated sediment-water mixtures, as well as fully saturated sediment-water mixture. As mentioned earlier in this thesis, unsaturated data from research in the field has not been thoroughly researched so finding comparative data was difficult, and finding only borehole data regarding T_2 and pore-size distribution data was difficult, this is also why the data in figure 29 was used as a comparison to the experimental borehole NMR data in this thesis. Nevertheless, the knowledge from [31] combined with my thesis could be used in combination in future research into unsaturated and fully saturated gravel-water mixtures and unconsolidated aquifers.
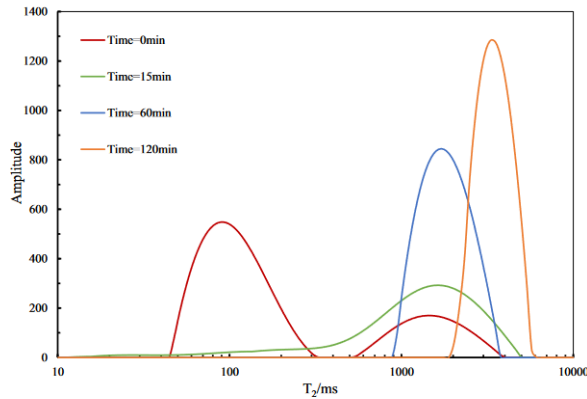
Fig. 4. T_2 distribution at different suffusion times.
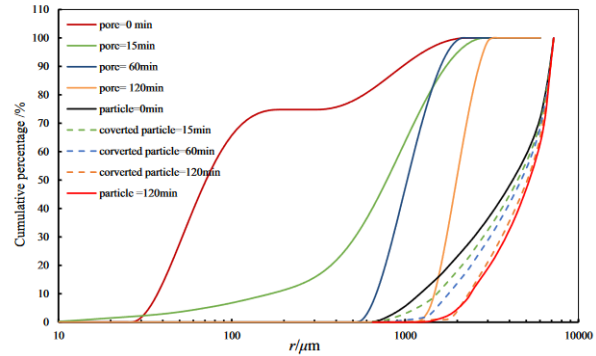
g. 5. Experimental results of pore size distribution and particle size distribution at different suffusion times.

(a) T_2 relaxation times of gravel-sand mixture. Image adapted from [31].

(b) Pore-size distributions of gravel sand mixture. Image adapted from [31].

Figure 29: Graphs showing NMR data from an experiment by a research group in China relating T_2 relaxation times and pore-size distributions of a gravel-sand mixture. Images adapted from [31].

Next, figure 30 shows data regarding the relaxation time T_2 and pore-size distribution of some sandstones from a research group in Japan [32]. The data in figure 30 was used as a comparison for the transverse relaxation time T_2 and pore-size distribution data in this thesis, regarding the experimental borehole NMR data, and transverse relaxation time T_2 from the rock analyzer results regarding sand. Quartz is a key component of sandstone and quartz is in sand so a comparison is valid between the data in figure 30 and my T_2 and pore-size distribution data sets. Also, sandstone is a consolidated material so comparing my T_2 and pore-size distribution data sets regarding sand which is in unconsolidated aquifers, it can be seen if unconsolidated and consolidated materials have similar NMR properties. Even though Minagawa et al [32] used lab NMR, they also wanted to measure the permeability in specifically methane hydrate-bearing sediments, so their method and set up was slighty different to mine, and this could be a reason for difference in their T_2, and pore-size distribution data compared to mine. As mentioned earlier in this thesis, unsaturated data from research in the field has not been thoroughly researched so finding comparative data was difficult, and finding only borehole data regarding T_2 and pore-size distribution data was difficult, this is also why the data in figure 30 was used as a comparison to the experimental borehole NMR data in this thesis. Nevertheless, the knowledge from [32] combined with my thesis could be used in combination in future research into unsaturated and fully saturated gravel-water mixtures and unconsolidated aquifers.

All of the T_2 borehole NMR data sets for the gravel sediments have relaxation curves in the range of 10^{-2}-10^1 s which is the range of the x-axis in figure 29a. My data sets have more relaxation curves also but there is at least a matching range for some of the T_2 values between my data sets and Feng et al [31]. Although, the signal amplitude is a lot smaller in my data sets compared to the y-axis of the data in figure 29a from Feng et al [31]. Similarly for my pore-size distribution data in figure 9, there are curves relating to signal magnitude which are in the same range, as the pore-size distribution data in figure 29b. The similarities between my gravel data and the data from Feng et al [31] show that despite slightly different methods and sediment mixtures, gravel sediments do exhibit similar values of T_2. No papers were found which exactly match the aim and experimental procedure performed in this thesis but the similarity between my results and some of the results from Feng et al in figure 29, show that gravel has similar NMR properties. For joint, lawn and quartz sand, all of the T_2 borehole NMR
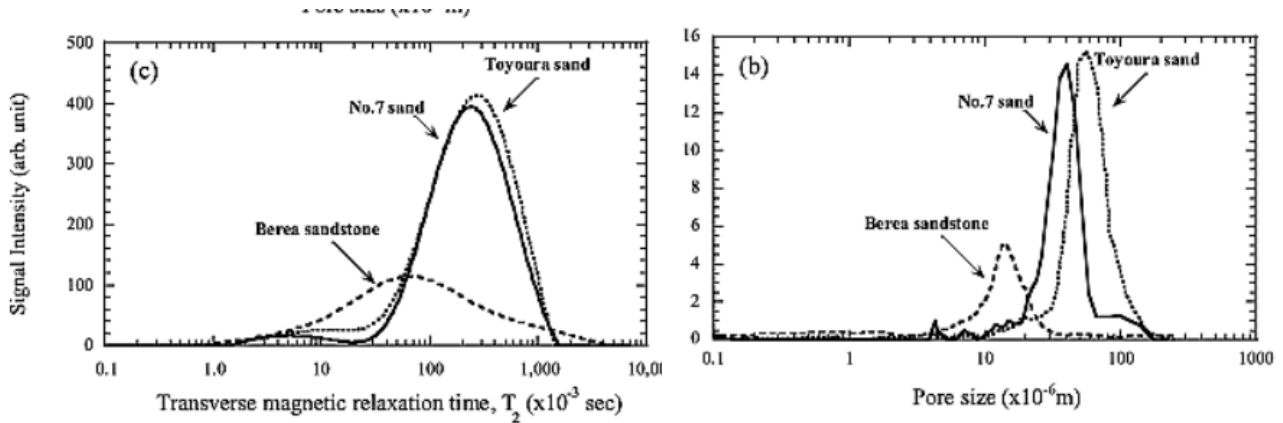
(a) T_2 relaxation time of different sandstones. Image adapted from [32].

(b) Pore-size distribution of different sandstones. Image adapted from [32].

Figure 30: Graphs showing data from an experiment by a research group in Japan relating relaxation time T_2 and pore size distribution of different sandstones. Images adapted from [32].

data sets have relaxation curves in the range of 10^{-4}-10^1 s which is the range of the x-axis in figure 30a. My data sets have more relaxation curves also but there is at least a matching range for some of the T_2 values between my data sets and Minagawa et al [32]. Although, the signal amplitude is a lot smaller in my data sets compared to the y-axis of the data in figure 30a from Minagawa et al [32]. Similarly for my pore-size distribution data in figure 12, there are curves relating to signal magnitude which are in the same range, as the pore-size distribution data in figure 30b. The similarities between my sand data and the data from Minagawa et al [32] show that despite slightly different methods and sand sediments, sand does exhibit similar values of T_2. Pehme et al found that the signal amplitude from water in clay-bound pores can decay very quickly (which indicates smaller pores) [10]. Pehme et al also found that the signal amplitude from water in capillary-bound (bound water) pores decays quickly [10]. Where as water in larger pores which is usually mobile water has a slower decaying signal for the T_2 spectra [10]. Based on figures 8a and 9 and 28 and using the reasoning by Pehme et al combined with the water regime boundaries from NUCLEUSinv, this could be interpreted to mean that the crushed marble stone and round/quartz gravel used in this thesis have small, medium and large pores present. Then, the water within the structure of these two gravel sediments is focused around the electrical double layer due to clay-bound pores [33], as well as water around the surrounding mineral surfaces due to capillary-bound (bound water) pores [34]. Where as the lawn quartz has no water around the electrical double layer due to no clay-bound pores [33] in figure 9. For the sand sediment data in figures 11a, 12 and 28, and using the reasoning by Pehme et al combined with the water regime boundaries from NUCLEUSinv, this could be interpreted to mean that joint sand and quartz sand used in this thesis have small, medium and large pores present. Then, the water within the structure of these two sands is focused around the electrical double layer due to clay-bound pores [33], as well as water around the surrounding mineral surfaces due to capillary-bound (bound water) pores [34]. Where as the lawn sand has no water surrounding mineral surfaces due to capillary-bound (bound water) pores [34] in figure 12.

Comparing the T_2 relaxation time borehole NMR data for the gravel and sand sediments, and comparing these data sets to the theoretical pore sizes in figure 28, it can be inferred each gravel and sand sediment has a distribution of pore sizes within their structures. This is the same conclusion from comparing my data to Feng et al [31] and Minagawa et al [32] in the previous paragraph. This is also

conferred by the data in figures 9 and 12 which shows a range of variation in the distribution of pore size and signal magnitude for the fully saturated gravel and sand sediments. According to theory, a fully saturated pore should have a single T_2 value [35], and this depends on the pore size where as multiple T_2 curves means there are multiple pores, and based on the pore-size distribution in figures 9 and 12, combined with figure 28, all the gravel and sand sediments in this thesis have different pore sizes. For the data sets regarding sand, every T_2 spectra as well as the pore-size distribution data in figure 12 have curves around similar values which indicates for joint, lawn and quartz sand despite the variation in particle size, have similar relaxation times and pore sizes of a certain value (around 10^{-5}-10^{-4} m) which is in a similar range to the larger pore sizes for the gravel sediments in figure 9. One reason why the pore-size distribution data is only shown for the fully saturated gravel and sand data set is because T_2 data sets of fully saturated materials usually have less anomalies than T_2 data sets of unsaturated materials. And, T_2 values are used in the process of calculating the pore-size, therefore the pore-size distribution data sets relating to figures 14a, 16a, 18a and 20a are not shown. An assumption which is commonly made in order to interpret NMR data is that the surface relaxivity (ρ) is constant [36]. An accurate value of ρ would lead to reasonable pore-size distribution [37]. Therefore, assuming ρ was determined correctly by the DART probe, the pore-size distribution data in figures 9 and 12 can be trusted. Unfortunately, with the equipment used, the actual value of ρ could not be seen, so this is why it must be assumed that it was measured accurately, and then the pore-size distribution data for gravel and sand in figures 9 and 12 can be considered accurate. There are also some interesting observations in the unsaturated gravel data sets. For example, in figure 14a (with $S_r \approx 0.500$) regarding the unsaturated lawn quartz, the signal magnitude increases from a value of $T_2 \approx 10^1$ s until the end of the graph, and this is not a common phenomenon with T_2 relaxation spectra. Similarly for the unsaturated crushed marble stone in figure 18a (with $S_r \approx 0.100$), there is a sharp increase in signal magnitude at the very end of the T_2 spectra where $T_2 \approx 10^2$ s. These are considered anomalies since these were not seen on other T_2 spectra, such as data by Feng et al [31] in figure 29a. Also, the T_2 relaxation time curves in figures 14a, 16a, 18a and 20a might be at smaller values of T_2, and offset a little [17] because these data sets represent data from unsaturated gravel and sand samples. This is another reason for not showing the pore-size distribution data for the unsaturated gravel and sand samples because the T_2 value could not be accurate. In general, materials with large pores have longer relaxation time [14], and Flinchum et al say gravel materials have larger pores. This means the curves around the values of $10^0 < T_2$ s in figures 8a and 11a lead to a conclusion that crushed marble stone, round/quartz gravel, lawn quartz, joint sand, lawn sand and quartz sand all have large pores within their pore structure combined with smaller sized pores too, combined with the pore-site distribution data in figures 9 and 12. Also, NMR is usually based on the hypothesis that the formation is homogeneous around the borehole, but pores and fluids can exhibit different properties around the borehole [25]. A non-homogeneous formation could mean the rocks are not homogeneous with depth and the radial direction but also around the borehole [25]. If the formation is not homogeneous, it can lead to errors in measurements. In this thesis, the borehole was set up to be as precise as possible. Technically, the borehole in this thesis was above ground and this could lead to experimental error because my borehole was made for this thesis, so it is not an 'actual' borehole because conventional boreholes are below the Earth's surface. Hence, the formation of the sediments in the borehole could not have been homogeneous. The T_2 borehole NMR data for the gravel and sand sediments, each sediment shows a difference in the T_2 spectra at a different saturation level, and/or there is sometimes an 'anomalous' increase in signal magnitude. This indicates the DART probe could be at fault because for each experiment, the sample of gravel or sand sediment was taken from the same bag. Another reason for differences in these T_2 data sets as well as random increase in signal magnitude could be due to saturation. When the sediment-water mixtures were created, the gravel or sand were mixed

with water in a bucket to get the desired degree of saturation. Due to experimental error there could be inhomogeneous saturation, i.e., every individual piece of crushed marble stone or grain of joint sand could have not been fully saturated, for the fully saturated data (for example), the same goes for other gravel and sand sediments. Then, for the unsaturated sediment-water mixtures, since these are not fully saturated, and using the reasoning from the previous sentence, these pieces of gravel or grains of sand could not even contain any water which would have made measuring the T_2 relaxation time and pore-size distribution even more difficult and less reliable. This could be the reason for the anomalous increases in signal magnitude of the unsaturated lawn quartz (with $S_r \approx 0.500$) in figure 14a, and unsaturated crushed marble stone (with $S_r \approx 0.100$) in figure 18a, the fully saturated quartz sand T_2 spectra in figure 11a , unsaturated joint sand (with $S_r \approx 0.500$ and 0.100) in figures 16a and 20a, and unsaturated lawn sand (with $S_r \approx 0.100$) in figure 20a. Also, it can be seen in all the decay curves for the gravel and sand borehole NMR data in figures 8b, 11b, 14b, 16b, 18b and 20 that there are more data points at at larger times, and less data points at shorter times. This was noticed in all the experiments and was interesting to observe. It could be due to the experimental set up as well. For example, during experiments the entire DART probe was not surrounded by the gravel or sand sediment. For each experiment the borehole was filled up to a height of 0.500 ± 0.001 m each time, so the upper half of the DART probe was not surrounded by any gravel or sand sediment. This experimental error could have lead to inaccurate measurements and therefore, the DART probe didn't pick measure more decaying data points at shorter values of time. Flinchum et al [14] found that magnetic gradients within the material can cause difficulty in measurements. These magnetic gradients causes the protons to oscillate at different larmor frequencies, and this variation in larmor frequency creates a more rapid decay signal [14]. It is concluded that all the gravel and sand sediments contained magnetic gradients. Another factor that should be taken into account is the NUCLEUSinv software, originally, the import process wouldn't work for my outputted data from the DART probe. Dr. Thomas Hiller was very helpful and created a separate upload process for my files. NUCLEUSinv is a free online software and currently does not have the exact optimization settings standardised or a manual [30], so another factor for the inversion not being perfect is due to the parameters I chose were not optimal. Muller et al found that the NMR relaxation times of fluids in porous media can be shortened due to influence of the pore wall [38]. This means the pore wall is able to interact with the protons whilst the spin's of the protons undergo relaxation. This influence of the pore wall mentioned by Muller et al is caused my local magnetic fields close to the pore surface [38]. This could mean that the relaxation times in figures 8a, 11a, 14a, 16a, 18a and 20a are shorter than normal which would lead the pore-sizes to be smaller than the actual true values. This means analysing NMR data from unconsolidated materials, like the sediments in this thesis more difficult because it is not known accurately if the pore wall has affected the data. Another phenomenon relating to the relaxation time found by Muller et al was the coarser the material the shorter the relaxation time [38]. Gravel counts as a coarse material, and sand is not according to [39]. Based on my findings, the T_2 spectra of the gravel sediments in figures 8a, 14a and 18a isn't necessarily at shorter T_2 values compared to the borehole NMR data for the sand sediments. Instead they have similar T_2 values. Therefore the statement of the coarser the material the shorter the relaxation time [38] is inconclusive from my borehole NMR data.

Regarding the all of the T_2 data sets from the rock analyzer, the gravel data sets have relaxation curves in the range of 10^{-2}-10^{1} s which is the range of the x-axis in figure 29a from Feng et al [31]. My T_2 data sets are similar to the data in figure 29a, in the sense that the relaxation curve of each gravel sediment is continuous and it is 'one' curve. As well as this, the signal amplitude is a similar order of magnitude in my data sets compared to the y-axis of the data in figure 29a. A reason why my data sets from the rock analyzer have a similar signal magnitude compared to the data in figure 29a, unlike

my borehole NMR data could be because the rock analyzer is essentially lab NMR, which is what Feng et al [31] used to get the data in figure 29a. For the rock analyzer data regarding joint, lawn and quartz sand, all of the T_2 data sets have relaxation curves in the range of 10^{-4}-10^1 s which is the range of the x-axis in figure 30a from Minagawa et al [32]. My T_2 data sets are similar to the data in figure 30a, in the sense that the relaxation curve of each gravel sediment is continuous and it is 'one' curve. Although, my data sets from the rock analyzer have a higher signal magnitude compared to the y-axis of the data in figure 30a. Nevertheless, the signal magnitude in figure 30a and my T_2 sand data sets from the rock analyzer are higher than the borehole NMR data sets. A reason why my data sets from the rock analyzer have a slightly higher signal magnitude compared to the data in figure 30a is because the method and research aim were also different as mentioned before. No papers were found which exactly match the aim and experimental procedure performed in this thesis but the similarity between my results and some of the results from Minagawa et al in figure 30, show that different types of sandstones and sands have similar NMR properties.

Comparing the T_2 relaxation time data from the rock analyzer for the gravel sediments, the fully saturated data set and unsaturated data set (with $S_r \approx 0.500$) show relaxation in a similar range of T_2 (10^{-2}-10^1 s). But the unsaturated T_2 spectra (with $S_r \approx 0.100$) has a completely different pattern, the range of T_2 relaxation is broader for each gravel sediment, and range is roughly 10^{-4}-10^0 s for round/quartz gravel and lawn quartz but shorter for the crushed marble stone (the range of $T_2 \approx 10^{-3}$-10^0 s). The overall signal magnitude of all gravel sediments on average also decreases as the degree of saturation decreases, particularly for the unsaturated marble (with $S_r \approx 0.100$) in figure 19 which could make sense because as the degree of saturation decreases, so does the amount of water in the sediment-water mixture. For the T_2 relaxation time data from the rock analyzer for the sand sediments, there is no clear similar shape or pattern between the spectra at different saturation levels. Similar to the rock analyzer T_2 spectra of the gravel sediments, the T_2 spectra of the sand sediments are not a similar shape to the borehole NMR data for the sand sediments. However, the range of T_2 relaxation values for the sand sediments always ends at $T_2 \approx 10^0$ s where as the curves start to increase in signal magnitude from different values T_2, $\approx 10^{-3}$ s for the fully saturated data in figure 13 , and $T_2 \approx 10^{-4}$ s for the unsaturated data sets in figures 17 and 21. In general, materials with large pores have longer relaxation time [14], and Flinchum et al say gravel materials have larger pores. This could explain the curves around $10^0 < T_2$ s in figures 10, 15. Using this logic would mean that crushed marble stone, round/quartz gravel and lawn quartz all have large pores within their pore structure combined with smaller sized pores too, based on figures 10, 15 which supports the earlier conclusion of a range of pore sizes in these sediments. In figures 13, 17, and 21, there are no curves with a value of $10^0 < T_2$ s. Using the reasoning from Flinchum et al logic would mean that joint, lawn and quartz sand all don't have have large pores within their pore structure, but instead smaller and medium sized pores. Also, the T_2 relaxation time curves in figures 15, 17, 19 and 21 might be at smaller values of T_2, and offset a little [17] because these data sets represent data from unsaturated gravel and sand samples. This is one reason why it is difficult to precisely and accurately analyse unsaturated NMR data sets because the T_2 relaxation time might not be completely accurate. Overall, the T_2 spectra of the gravel and sand sediments differs between the rock analyzer and borehole NMR data. This could be due to pore-coupling (which apparently was not showed from the T_2 spectra in the borehole NMR data). Based on figures and information from Wang et al [40] as well as a Master thesis completed in 2022 from my research group [41]. Some of the rock analyzer T_2 spectra of the gravel and sand sediments in figures 10, 13, 15,17, 19 and 21 could look as they do because of pore coupling, which means the interpretation of these graphs is more difficult. For example, the spectra all the fully saturated gravel sediments, and unsaturated gravel sediments (with $S_r \approx 0.500$) show potential pore-coupling.

As well as the spectra all the joint sand, and lawn sand T_2 spectra show potential pore-coupling. The quartz sand spectra could also be the shape it is due to pore coupling but it is hard to determine for definite. The 'small bumps' in the curves which precede the larger curves from some of the rock analyzer spectra for the gravel sediments are an anomaly area according to data from [40] who used NMR in siliciclastic carbonate rocks, and carbonate rocks could have more pore coupling compared to non-carbonate rocks [42]. The reason why the interpretation of the pore-size distribution would be difficult from figures 10 and 13 is because if the pore-size distribution graph would have the exact same shape as the T_2 spectra (like with the borehole NMR data) then it would be hard to concretely say what the exact pore size of the gravel sediments would be. Where as the pore-size distribution spectra of the gravel and sand sediments in figures 9 and 12 shows curves which increase from 0 and decrease back to 0 in signal magnitude, and these curves are centered around certain pore size values. As mentioned before, an assumption which is commonly made in order to interpret NMR data is that the surface relaxivity is constant [36], but surface geochemistry is one factor that can control pore coupling [41], and surface relaxivity is part of the surface geochemistry. And, overall is concluded from my measurements from the rock analyzer, it is concluded that the gravel and sand samples measured had pore coupling. On the other hand, a reason for saying the results from the rock analyzer should be focused on more than the borehole NMR data is because the magnetic field is weaker when using borehole NMR compared to lab NMR [10]. This is due the rock/sediment being outside of the source in borehole NMR compared to lab NMR [10]. One research group found that the NMR relaxation times of fluids in porous media can be shortened due to influence of the pore wall, as found by Muller et al [38]. This influence of the pore wall mentioned by Muller et al is caused my local magnetic fields close to the pore surface [38]. This could mean that the relaxation times in figures 10, 13, 15,17, 19 and 21 are shorter than normal. Another phenomenon relating to the relaxation time found by Muller et al was the coarser the material the shorter the relaxation time [38]. Gravel counts as a coarse material, and sand is not according to [39]. Based on my findings, the T_2 spectra of the gravel sediments in figures 10, 15 and 19 isn't necessarily at shorter T_2 values compared to the data from the rock analyzer for the sand sediments in figures 13, 17 and 21, but instead they have similar T_2 values. Even for the fully saturated and unsaturated gravel data in figures 10 and 15, it could be argued the T_2 values of the gravel sediments are slightly larger than some of the T_2 values for the from the rock analyzer data. Therefore, the statement of the coarser the material the shorter the relaxation time [38] is inconclusive from my data sets obtained from the rock analyzer.

Comparing the hydraulic conductivity (K) estimates from borehole NMR for the gravel and sand sediments, the SOE estimates of K are all in the range of 10^2- 10^3 m/day for all the sediments, which is in the range of values for gravel and sand according to [43]. Also, compared to other research groups who measured K in aquifers, for example, the range of my estimates of K are similar to the ranges of measured values such as Dlubac et al [44]. The authors of this paper determined hydraulic conductivity in boreholes in the high plains acquirer in the US which is unconsolidated, and the geology of the boreholes they used contained gravel and sand, as well as gravel/sand mixtures, which are the measured materials in this thesis. Dlubac et al wanted to see if NMR logging estimates of K were reliable, and they used the SDR and TC estimates which are also what the DART probe use. The authors assumed the borehole was fully screened (which means no sand or gravel could collapse into the borehole). However, in this thesis, in every experiment performed using the DART probe, sediments were touching the DART probe which in reality doesn't usually happen as seen in figure 2. This being said, since my borehole was not 'screened' in any experiment, it is a controlled variable so the error of sediments touching the DART probe is fair, since it occurred in every experiment. However, all the estimates of K in figures 22a, 23a, 24a, 25a, 26a and 27a are from experimental data,

and singh et al found that experimental estimates of K can not be directly compared to field data, for example, to aquifers [8]. And, currently researchers are looking for alternative methods to calculate hydraulic conductivity in the field [8], so the values from the DART probe which are experimental do tell us values about gravel and sand sediments, but only experimentally. This is acceptable because one reason motivating this thesis is to 'test' the DART probe and see how it functions and the results it produces. For interpreting the results of estimates of K, I have focused on the SOE estimate of K compared to the SDR and TC estimates. One reason why is because it is difficult to make a comparison between the SDR & and TC estimates of K from figures 22a, 23a, 24a, 25a, 26a and 27a because the relationship between the SDR and TC estimates of K and depth of the borehole change infrequently and at different values. Also, the range of K on the x-axes in my figures is small where as the data found by Dlubac et al in [44] who measured hydraulic conductivity in an aquifer in the US, the range of K is 10^{-11} m/s- 10^{-2} m/s [(8.64 x 10^{-7})-864 m/day], and this upper limit is on my data sets, but the lower limit on my data sets is generally larger than the lower limit of 10^{-11} m/s used by Dlubac et al [44]. Another reason I have not discussed the SDR and TC estimates in detail is because from research in the field, SDR and TC estimates of K and can fluctuate rapidly, as seen by Dlubac et al [44]. This could be a reason for the great variation of the SDR and TC estimates of K with depth of the borehole in this thesis. On the other hand, it is generally acceptable for estimates of K to vary by 1 order of magnitude in the same test [27] due to many acquisition parameters. However, as can be seen from the SDR and TC estimates of K in my data sets, it seems like most of the time the SDR and TC estimates are changing potentially by more than one magnitude (particularly the TC estimates) but this can not be confirmed due to the scale of the x-axis. Not many papers were found which used the SOE method to estimate hydraulic conductivity in boreholes so it was difficult to find authors who have performed similar research and directly compare my SOE estimates of K with theirs. Also, multiple research groups found SDR estimates of K in semi/full unconsolidated aquifers were not accurate using constants from sandstone [45] [27]. The materials used in this thesis were gravel and sand which compose the formation of unconsolidated aquifers. This is another reason why the SOE estimates of K were looked at more closely compared to the SDR estimate, because the DART probe uses constants from consolidated sandstone. A significant finding by Knight et al found SDR estimates barely differed between sights [45] and these authors performed measurements in an unconsolidated aquifer. The SOE estimates of K in my data sets also barely differ which is a similar pattern to Knight et al. Despite being a different type of estimate, the similar relationship between K and depth of the borehole between my SOE estimates and the SDR estimates of Knight et al could be due to the factor of unconsolidated aquifer. Because the materials that I have used in this thesis form unconsolidated aquifers. Linking to this is data from Parsekian et al, and they measured hydraulic conductivity in an unconsolidated fluvial aquifer in Kansas [46] and their values were within a range of roughly 10^{-4}-10^{-3} m/s, with many measurements having a magnitude of 10^{-3} m/s. Converting this to metres/day which are the units of K from the DART probe, the range is 8.64-86.4 m/day. This range is roughly 10^1-10^2 m/day, so these values would not be shown by the DART and the values found by Parsekian et al seem to be an order of 10 magnitude lower than my results [46]. This being said, Parsekian et al were not surprised that many estimates of K had similar values because the authors performed measurements in the same aquifer system [46]. This supports the trend of SOE estimates of K from my data sets that the range is 10^2-10^3 m/day for every sediment, because I performed all of my measurements in the same system of a 'experimental' borehole. Although, during all my experiments, the sediments were touching the DART probe constantly, and in an ideal borehole this does not happen. Finally, The SOE estimates of K values for all of my data sets are within the range of values that an American research group found from their research [47]. Most values of K found by Landon et al were in between 10^2-10^3 m/day. The authors performed

measurements of hydraulic conductivtity in salty steameds which were composed of sand and gravel so, the sediments that were used in this thesis could have been in the measurement area of Landon et al [47]. The similarity between estimates of K measured by the DART probe in this thesis of different types of gravel and sand indicated that the DART probe is a great tool to use in the field. A reason for the slight difference in K estimates (particularly for the SDR and TC estimates) between the sediments could be due to the variation of surface relaxivity [38]. As mentioned before, the estimates of K form the unsaturated gravel & sand sediment are not presented in this thesis, although they were recorded. Measuring hydraulic conductivity in unsaturated zones can be more difficult compared to fully saturated zones because sometimes in unsaturated rocks or soil, the water is actually moisture since it is sparser in unsaturated conditions compared to a saturated conditions. For example, one research group used NMR in the vadose zone, and found that K vs moisture content relationships in unsaturated conditions are non linear and can have a memory effect known as hysteresis [48]. This relationship depends on how the moisture partitions between pores of different sizes as well as soil composition and texture [48]. And, as seen from the saturated gravel and sand pore-size distribution data sets in figures 9 and 12, the sediments measured in this thesis potentially have a range of pore sizes. Combined with the discovery of Roy et al [48], are findings from the US Geological Survey which found the values of hydraulic conductivity measured for unsaturated rocks can be less accurate [12]. Specifically the previous sentence relates to rocks but the gravel sediments used in this thesis are stones and the crushed marble stone, as well as round/quartz gravel originate from a rock. Therefore, the unsaturated estimates of K were not used for the gravel sediments and to keep the discussion fair, also the unsaturated K estimates from the sand sediments will not presented. Also, as soil pores become more de-saturated, they empty and the value of hydraulic conductivity decreases significantly, and the estimates of hydraulic conductivity in unsaturated soil are always orders of magnitudes less compared to when the soil is fully saturated [49]. Overall, incorporating these reasons together shows that the fully saturated gravel K estimates should be focused on more compared to the unsaturated estimates of K.

Regarding the water content estimates by the DART probe for the borehole NMR data, all data sets in figures 22b, 23b, 24b, 25b, 26b and 27b show different patterns of clay and capillary water but overall, mobile water was the most present water regime in each sediment. One reason for the reliability of these results is because Schmidt and Rumpe found that there are detectable differences in measured water content from using NMR at shallow depths [2]. The borehole used in this thesis was very shallow, with a depth of 0.500 ± 0.001 m, so all of the borehole NMR data measured by the DART probe was performed in shallow depths. Relatively, a depth of 0.500 ± 0.001 m is very, very small for a borehole. On the other hand, the borehole used in this thesis was self-made and above ground but nevertheless, the set up was controlled. The water content estimates of each sediment showing different distributions of each water regime could also be accurate because another research group found that different fine-grained units in a sample have different types of water, namely clay and capillary water [10]. On the contrary, the fact that there was mobile water present at all depths of the borehole for all the water content data sets leads to a question of, is this a characteristic of the DART probe or was there actually mobile water present everywhere? Perhaps, due to the sediment touching the DART probe during the whole experiment, and since it was a fully saturated sediment-water mixture, this could mean wet sediment was touching the DART probe the whole time during each experiment. Therefore, the DART probe could have interpreted this as mobile water. Although, Pehme et al found that water in larger pores which is usually mobile water has a slower decaying signal for the T_2 spectra [10]. Linking this to the pore-size of each sediment, this could mean that the presence of mobile water in all the water content data sets indicate that all the gravel and sand sediments measured in this

thesis have large pores And, using theory from figure 28, it does mean some of the results from this thesis indicate large pores. On the other hand, also according to Pehme et al, features of a rock thinner than minimum identifiable aperture would not be detected due to the resolution of the tool [10], and the fluid detected would appear as free water (mobile water) in terms of the total water content [10]. Pehme et al also noted that the signal amplitude from water in clay-bound pores and capillary-bound (bound water) pores can decay very quickly (which indicates smaller pores) [10]. Using this interpretation would mean that lawn quartz and lawn sand barely have any small pores based on their water content data sets since there is not a lot of clay or bound water in figures 24b and 26b. Although, the fully saturated lawn sand sample in figure 12 does have a small pore size around 10^7 m but the signal magnitude is very small. Also, knowing the water content layout in unconsolidated boreholes is good for developing empirical constants for estimating hydraulic conductivity [10]. Therefore, the hydraulic conductivity and water content estimates from this thesis combined with future research could be combined for trying to find the optimal equation for calculating hydraulic conductivity in unconsolidated aquifers. so the experimental data from the DART probe gathered in this thesis shows that regardless of particle size, mobile water is present at all depths of a shallow borehole when filled with different types of gravel and sand.

For the derived water content values from the rock analyzer in table 3, there was noise in every experiment. This was known because when forming the linear regression equation of a line, it was noticed that the 'MaxPeak' value for the standard sample which had 0 water content, was a non-zero number. The 'MaxPeak' value should be 0 for the standard sample with 0 grams of water but evidently this was not the case. Also, the rock analyzer is conventionally used to measure and analyze core samples taken from the field, but in this thesis, small stones of gravel and grains of sand were placed into the sample holder, which was placed into the core holder. This difference in structure of the sample could be a reason for the abnormal high water content values in table 3. Also, the same 'calibration equation' had to be used for each saturation level for the same sediment to make comparisons fair, i.e., the same equation of a line to calculate the water content in the crushed marble stone had to be used for three measured saturation levels. Regarding lawn sand, the particle size has a bigger range compared to the other types of sand used in this thesis. So, it makes sense lawn sand should be able to hold more water (assuming the pores are bigger) but the value of 20.541 grams of water for the saturated sample is really obscure since the wet mass used was much smaller than this (see appendix B.1). This could indicate that lawn sand can hold a more water than joint sand and quartz sand which leads to a conclusion that the pores are larger in lawn sand compared to joint sand and quartz sand. Regarding lawn quartz, the particle size was the smallest out of the gravel sediments used in this thesis, so it is strange that the saturated lawn quartz had the highest water content (despite being very high anyway) compared to the fully saturate crushed marble stone and round/quartz gravel samples (assuming some of the lawn quartz pores are be smaller). The value of 14.075 grams of water for the saturated lawn quartz sample is really obscure since the wet mass used was much smaller than this (see appendix B.1). Another reason for the interesting results in table 3 could be due to inhomogeneous saturation. When the sediment-water mixtures were created, the gravel and sand sediments were mixed with water in a bucket to get the desired degree of saturation. Due to experimental error there could be inhomogeneous saturation, i.e., every individual piece of crushed marble stone could have not been fully saturated, for the fully saturated data (for example), the same goes for the other fully saturated sediment-water mixtures. Then, for the unsaturated mixtures, since these are not fully saturated, and using the reasoning from the previous sentence, the pieces of gravel or grains of sand could have not even contained any water which would have made measuring the T_2 relaxation time less reliable. The 'MaxPeak' value from each experiment is determined from

the T_2 relaxation time, which means the 'MaxPeak' of the signal could be inaccurate (using the reasoning from the previous sentence) which would lead to inaccurate derived water content values. Hence, this could be the reason for the high values of water content in table 3. Overall, the water content values in table 3 are considered not accurate but the general trend was hypothesised before the experiment, i.e., as saturation level increases, so does the water content.

6   Conclusion

6.1   Conclusion

The aim of this thesis was to measure various hydrogeologic properties, namely: the transverse relaxation time (T_2), pore-size distribution, hydraulic conductivity (k) and water content of different sediments in saturated and unsaturated conditions to see how saturation level affects these properties. Combined with producing data which can be used in comparison with data in the field for unconsolidated aquifers. As well as observing the use of a newly acquired DART probe and rock analyzer to examine the operational capacity. In this thesis three types of gravel and three types of sand were measured, namely: crushed marble stone, round7quartz gravel, lawn quartz, joint sand, lawn sand and quartz sand. The data presented in this thesis gives a detailed overview into different hydrogeologic properties measured in, gravel-water and sand-water mixtures. Saturated and unsaturated sediment-water mixtures were formed, and as can be seen from the data, the type of sediment and saturation level affects the transfer and storage properties. Evidently, the T_2 and pore-size distribution data combined with theory show a range of pore sizes within each sediment. The NUCLEUSinv program is a good program to use in order to interpret T_2 and pore-size distribution data but make sure to become familiar with the software. The DART probe from Vista Clara produced similar estimates for hydraulic conductivity for every sediment but these values do fall into the range of accepted values for hydraulic conductivity. Last but not least, the water content data from the DART probe showed some difference between the sediments in terms of quantities of clay, capillary and mobile water. For the T_2 relaxation time data from the rock analyzer, there was some similarity between these results and the T_2 results from the experiments using the DART probe. The transverse relaxation curves produced by the rock analyzer were more continuous compared to the T_2 data from the DART probe, and the rock analyzer indicated some pore coupling effects which was not picked up by the DART probe. Overall, the DART probe from Vista Clara, and the rock analyzer did in operate in acceptable capacity.

6.2   Outlook

Perhaps, for future research and development in the world of SNMR and borehole NMR, more research can be completed in the area of biophysics. The use of nuclear magnetic resonance in biophysics is emerging and as a research community, we could use NMR to measure the Geophysical signatures of microbial interactions with geological media [50]. Also, understanding geophysical features which are linked to microbes and microbial interactions has potential in microbial oil recovery [13]. Regarding borehole NMR, more research is needed in unsaturated rocks which has been started by one group [2]. I performed a lot of experiments using unsaturated sediment-water mixtures but my samples were not rocks but instead sediments, so I would recommend performing more measurements in the field. From the research in this thesis, borehole NMR can suffer from a significant signal-to-noise ratio and materials with high magnetic susceptibilities, as also found by this group [2]. Also, magnetic inhomogeneities in the magnetic field used for NMR measurements is a possible downfall to NMR, but increasing research in this field will lead to better results and more understanding of how to counteract this fault when performing measurements. Finally, the results from this thesis can be used in comparison with research from the field field which specifically examine unconsolidated aquifers, in order to gain a more definitive insight into transfer and storage properties of unconsolidated aquifers.

6.3   Conflicts of interest

There are no conflicts of interest to declare.

Bibliography

[1] Rajat Kango, Vijay Shankar, and MA Alam. Evaluation of hydraulic conductivity based on grain size distribution parameters using power function model. *Water Supply*, 19(2):596–602, 2019.

[2] Logan Schmidt and Daniella Rempe. Quantifying dynamic water storage in unsaturated bedrock with borehole nuclear magnetic resonance. *Geophysical Research Letters*, 47(22):e2020GL089600, 2020.

[3] Sean Cheong Heng Lee, Khairul Arifin Mohd Noh, and Muhammad Noor Amin Zakariah. High-resolution electrical resistivity tomography and seismic refraction for groundwater exploration in fracture hard rocks: A case study in kanthan, perak, malaysia. *Journal of Asian Earth Sciences*, 218:104880, 2021.

[4] AF McClymont, M Hayashi, LR Bentley, and J Liard. Locating and characterising groundwater storage areas within an alpine watershed using time-lapse gravity, gpr and seismic refraction methods. *Hydrological Processes*, 26(12):1792–1804, 2012.

[5] Rosli Saad, MNM Nawawi, and ET Mohamad. Groundwater detection in alluvium using 2-d electrical resistivity tomography (ert). *Electronic Journal of Geotechnical Engineering*, 17:369–376, 2012.

[6] Erwan Gloaguen, Michel Chouteau, Denis Marcotte, and Robert Chapuis. Estimation of hydraulic conductivity of an unconfined aquifer using cokriging of gpr and hydrostratigraphic data. *Journal of Applied Geophysics*, 47(2):135–152, 2001.

[7] Ugur Yaramanci and Mike Muller-Petke. Surface nuclear magnetic resonance—a unique tool for hydrogeophysics. *The leading edge*, 28(10):1240–1247, 2009.

[8] Uttam Singh and Pramod Kumar Sharma. Comparison of saturated hydraulic conductivity estimated by surface nmr and empirical equations. *Journal of Hydrology*, 617:128929, 2023.

[9] O Mohnke and U Yaramanci. Pore size distributions and hydraulic conductivities of rocks derived from magnetic resonance sounding relaxation data using multi-exponential decay time inversion. *Journal of Applied Geophysics*, 66(3-4):73–81, 2008.

[10] Peeter Pehme, Heather Crow, Beth Parker, and Hazen Russell. Evaluation of slim-hole nmr logging for hydrogeologic insights into dolostone and sandstone aquifers. *Journal of Hydrology*, 610:127809, 2022.

[11] Robert P Chapuis. Estimating the in situ porosity of sandy soils sampled in boreholes. *Engineering geology*, 141:57–64, 2012.

[12] Kim S Perkins. Measurement and modeling of unsaturated hydraulic conductivity. *Hydraulic Conductivity–Issues, Determination and Applications, Intech, China*, pages 419–434, 2011.

[13] Ahmad A Behroozmand, Kristina Keating, and Esben Auken. A review of the principles and applications of the nmr technique for near-surface characterization. *Surveys in geophysics*, 36(1):27–85, 2015.

[14] Brady A Flinchum, W Steven Holbrook, Andrew D Parsekian, and Bradley J Carr. Characterizing the critical zone using borehole and surface nuclear magnetic resonance. *Vadose Zone Journal*, 18(1):1–18, 2019.

[15] Kathryn E Washburn. Relaxation mechanisms and shales. *Concepts in Magnetic Resonance Part A*, 43(3):57–78, 2014.

[16] Thomas Hiller and Norbert Klitzsch. Joint inversion of nuclear magnetic resonance data from partially saturated rocks using a triangular pore model. *Geophysics*, 83(4):15–28, 2018.

[17] Mahmoud Elsayed, Abubakar Isah, Moaz Hiba, Amjed Hassan, Karem Al-Garadi, Mohamed Mahmoud, Ammar El-Husseiny, and Ahmed E Radwan. A review on the applications of nuclear magnetic resonance (nmr) in the oil and gas industry: laboratory and field-scale measurements. *Journal of Petroleum Exploration and Production Technology*, pages 1–38, 2022.

[18] Robert L Kleinberg and Jasper A Jackson. An introduction to the history of nmr well logging. *Concepts in Magnetic Resonance*, 13(6):340–342, 2001.

[19] Aytekin Timur. Pulsed nuclear magnetic resonance studies of porosity, movable fluid, and permeability of sandstones. *Journal of Petroleum Technology*, 21(06):775–786, 1969.

[20] LR Stingaciu, L Weihermüller, S Haber-Pohlmeier, S Stapf, H Vereecken, and A Pohlmeier. Determination of pore size distribution and hydraulic properties using nuclear magnetic resonance relaxometry: A comparative study of laboratory methods. *Water resources research*, 46(11), 2010.

[21] Thomas Hiller, Stephan Costabel, Tino Radić, Raphael Dlugosch, and Mike Müller-Petke. Feasibility study on prepolarized surface nuclear magnetic resonance for soil moisture measurements. *Vadose Zone Journal*, 20(5):e20138, 2021.

[22] Rosemary Knight, Elliot Grunewald, Trevor Irons, Katherine Dlubac, Yiqiao Song, Henry N Bachman, Ben Grau, Dave Walsh, Jared D Abraham, and Jim Cannia. Field experiment provides ground truth for surface nuclear magnetic resonance measurement. *Geophysical Research Letters*, 39(3), 2012.

[23] David Walsh, Peter Turner, Elliot Grunewald, Hong Zhang, James J Butler Jr, Ed Reboulet, Steve Knobbe, Tom Christy, John W Lane Jr, Carole D Johnson, et al. A small-diameter nmr logging tool for groundwater investigations. *Groundwater*, 51(6):914–926, 2013.

[24] Mike Müller-Petke, Thomas Hiller, Rolf Herrmann, and Ugur Yaramanci. Reliability and limitations of surface nmr assessed by comparison to borehole nmr. *Near Surface Geophysics*, 9(2):123–134, 2011.

[25] Guangzhi Liao, Sihui Luo, and Lizhi Xiao. Borehole nuclear magnetic resonance study at the china university of petroleum. *Journal of Magnetic Resonance*, 324:106914, 2021.

[26] USGS. Unconsolidated and semiconsolidated sand and gravel aquifers, March 2021. Last Accessed 4th June 2023.

[27] Katherine Isis Dlubac. *The relationship between nuclear magnetic resonance and permeability in near-surface unconsolidated materials*. Stanford University, 2013.

[28] Vista Clara Inc. Magnetic resonance borehole logging tools, September 2022. Last Accessed 3rd October 2022.

[29] Vista Clara. *DART manual and documentation*. Vista Clara, Inc, 2016.

[30] Thomas Hiller. Thohiller/nmr-nucleus: v0.1.13 (version v0.1.13), August 2022. Last Accessed 26th June 2023.

[31] Shangxin Feng, Zengguang Xu, Junrui Chai, and Yanlong Li. Using pore size distribution and porosity to estimate particle size distribution by nuclear magnetic resonance. *Soils and Foundations*, 60(4):1011–1019, 2020.

[32] Hideki Minagawa, Yasunori Nishikawa, Ikuko Ikeda, Kuniyuki Miyazaki, Naoya Takahara, Yasuhide Sakamoto, Takeshi Komai, and Hideo Narita. Characterization of sand sediment by pore size distribution and permeability using proton nuclear magnetic resonance measurement. *Journal of Geophysical Research: Solid Earth*, 113(B7), 2008.

[33] Schlumberger Limited. Clay-bound water, 2022. Last Accessed 9 September 2022.

[34] Wikipedia. Bound water, September 2022. Last Accessed 9th September 2022.

[35] George Coates, Lizhi Xiao, and Mannfred Prammer. *NMR principles logging and applications*. Halliburton energy services publication, 1999.

[36] Kristina Keating and Rosemary Knight. The effect of spatial variation in surface relaxivity on nuclear magnetic resonance relaxation rates. *Geophysics*, 77(5):E365–E377, 2012.

[37] Peiqiang Zhao, Liang Wang, Chenhao Xu, Jinhua Fu, Yujiang Shi, Zhiqiang Mao, and Dianshi Xiao. Nuclear magnetic resonance surface relaxivity and its advanced application in calculating pore size distributions. *Marine and Petroleum Geology*, 111:66–74, 2020.

[38] Martin Müller, Stefan Kooman, and Ugur Yaramanci. Nuclear magnetic resonance (nmr) properties of unconsolidated sediments in field and laboratory. *Near Surface Geophysics*, 3(4):275–285, 2005.

[39] McLanahan. Everything you need to know about coarse materials, June 2022. Last Accessed 5th July 2023.

[40] Mengqi Wang, Jun Xie, Fajun Guo, Yawei Zhou, Xudong Yang, and Ziang Meng. Determination of nmr t2 cutoff and ct scanning for pore structure evaluation in mixed siliciclastic–carbonate rocks before and after acidification. *Energies*, 13(6):1338, 2020.

[41] Francisca Antonia Soto Bravo. The nuclear magnetic resonance investigation of pore coupling effects in near-surface environments. Master's thesis, University of Vienna, 2022.

[42] Francisca Antonia Soto Bravo and Chi Zhang. A critical mini-review on the low-field nuclear magnetic resonance investigation of pore coupling effects in near-surface environments. *Vadose Zone Journal*, 1(1):1–12, 2022.

[43] Glenn M Duffield. Representative values of hydraulic properties, May 2023. Last Accessed 10th May 2023.

[44] Katherine Dlubac, Rosemary Knight, Yi-Qiao Song, Nate Bachman, Ben Grau, Jim Cannia, and John Williams. Use of nmr logging to obtain estimates of hydraulic conductivity in the high plains aquifer, nebraska, usa. *Water Resources Research*, 49(4):1871–1886, 2013.

[45] Rosemary Knight, David O Walsh, James J Butler Jr, Elliot Grunewald, Gaisheng Liu, Andrew D Parsekian, Edward C Reboulet, Steve Knobbe, and Mercer Barrows. Nmr logging to estimate hydraulic conductivity in unconsolidated aquifers. *Groundwater*, 54(1):104–114, 2016.

[46] AD Parsekian, K Dlubac, E Grunewald, JJ Butler, R Knight, and DO Walsh. Bootstrap calibration and uncertainty estimation of downhole nmr hydraulic conductivity estimates in an unconsolidated aquifer. *Groundwater*, 53(1):111–121, 2015.

[47] Matthew K Landon, David L Rus, and F Edwin Harvey. Comparison of instream methods for measuring hydraulic conductivity in sandy streambeds. *Groundwater*, 39(6):870–885, 2001.

[48] J Roy and M Lubczynski. Mrs multi-exponential decay analysis: Aquifer pore-size distribution and vadose zone characterization. near surface geophysics, 3, 287-298. *Crossref Web of Science*, 2005.

[49] Meter environment. How to measure soil hydraulic conductivtity, January 2022. Last Accessed 4th July 2023.

[50] Estella A Atekwana and Lee D Slater. Biogeophysics: A new frontier in earth science research. *Reviews of Geophysics*, 47(4), 2009.

Appendices

Different levels of saturation were measured, the first was $S_r = 1.000$, then $S_r = 0.500$, and finally $S_r = 0.100$. The degree of saturation for each experiment wasn't exactly at these values due to measurement error but the true degree of saturation for each experiment only deviates from these values by a very small amount.

A   Borehole NMR

Listed below are the inputs for the DART probe and the mass used of each sediment for every experiment performed in borehole NMR conditions. The values of scan length, recovery time, and number of averages were assigned by the DART probe and kept constant for each experiment so each experiment was controlled and fair, as well as for valid comparability of each experiment. The user manual recommends not to change these values unless one is an expert with the probe, hence for this thesis they were not altered.

The table below shows the inputs for the DART probe, and these values were kept the same for each experiment to make them fair and controlled.

Scan length [seconds]	Recovery time $T_r[seconds]$	Number of averages
0.2	2.0	50
0.02	0.1	300

A.1   Fully saturated data $S_r = 1.000$

Crushed marble stone: The calculated minimum mass of wet crushed marble stone needed was 12.076 kg, when using a dry mass of 7.500 kg. In reality, a wet mass of 12.115 ± 0.0005 kg was used from a dry mass of 7.514 ± 0.0005 kg. Hence, the actual value of S_r in this experiment was 1.007 ± 0.028.

Round/Quartz gravel: The calculated minimum mass of wet round/quartz gravel was 11.540 kg, when using a dry mass of 7.500 kg. In reality, a wet mass of 11.562 ± 0.0005 kg was used from a dry mass of 7.514 ± 0.0005 kg. Hence, the actual value of S_r in this experiment was 1.004 ± 0.031.

Lawn quartz: The calculated minimum mass of wet lawn quartz was 10.987 kg, when using a dry mass of 7.500 kg. In reality, a wet mass of 11.001 ± 0.0005 kg was used from a dry mass of 7.521 ± 0.0005 kg. Hence, the actual value of S_r in this experiment was 1.002 ± 0.036.

Joint sand: The calculated minimum mass of wet sand needed for each experiment had to be 13.006 kg, when using a dry mass of 7.500 kg.

In reality, a wet mass of 13.092 ± 0.0005 kg was used from a dry mass of 7.505 ± 0.0005 kg. Hence, the actual value of S_r in this experiment was 1.015 ± 0.023.

Lawn sand: In reality, a wet mass of 13.035 ± 0.0005 kg was used from a dry mass of 7.503 ± 0.0005 kg. Hence, the actual value of S_r in this experiment was 1.005 ± 0.023.

Quartz sand: In reality, a wet mass of 13.026 $\pm$ 0.0005 kg was used from a dry mass of 7.505 $\pm$ 0.0005 kg. Hence, the actual value of S_r in this experiment was 1.003 $\pm$ 0.023.

A.2   Unsaturated data S_r = 0.500

Crushed marble stone: The calculated minimum mass of wet crushed marble stone was 9.788 kg, when using a dry mass of 7.500 kg. In reality, a wet mass of 9.833 $\pm$ 0.0005 kg was used from a dry mass of 7.524 $\pm$ 0.0005 kg. Hence, the actual value of S_r in this experiment was 0.506 $\pm$ 0.014.

Round/Quartz gravel: The calculated minimum mass of wet round/quartz gravel was 9.520 kg, when using a dry mass of 7.500 kg. In reality, a wet mass of 9.529 $\pm$ 0.0005 kg was used from a dry mass of 7.507 $\pm$ 0.0005 kg. Hence, the actual value of S_r in this experiment was 0.501 $\pm$ 0.015.

Lawn quartz: The calculated minimum mass of wet lawn quartz was 9.243 kg, when using a dry mass of 7.500 kg. In reality, a wet mass of 9.293 $\pm$ 0.0005 kg was used from a dry mass of 7.517 $\pm$ 0.0005 kg. Hence, the actual value of S_r in this experiment was 0.511 $\pm$ 0.018.

Joint sand: The calculated minimum mass of wet sand needed for each experiment had to be 10.253 kg, when using a dry mass of 7.500 kg.

In reality, a wet mass of 10.273 $\pm$ 0.0005 kg was used from a dry mass of 7.511 $\pm$ 0.0005 kg. Hence, the actual value of S_r in this experiment was 0.502 $\pm$ 0.011.

Lawn sand: In reality, a wet mass of 10.275 $\pm$ 0.0005 kg was used from a dry mass of 7.513 $\pm$ 0.0005 kg. Hence, the actual value of S_r in this experiment was 0.502 $\pm$ 0.011.

Quartz sand: In reality, a wet mass of 10.273 $\pm$ 0.0005 kg was used from a dry mass of 7.511 $\pm$ 0.0005 kg. Hence, the actual value of S_r in this experiment was 0.502 $\pm$ 0.011.

A.3   Unsaturated data S_r = 0.100

Crushed marble stone: The calculated minimum mass of wet crushed marble stone was 7.958 kg, when using a dry mass of 7.500 kg. In reality, a wet mass of 7.985 $\pm$ 0.0005 kg was used from a dry mass of 7.500 $\pm$ 0.0005 kg. Hence, the actual value of S_r in this experiment was 0.106 $\pm$ 0.003.

Round/Quartz gravel: The calculated minimum mass of wet round/quartz gravel was 7.904 kg, when using a dry mass of 7.500 kg. In reality, a wet mass of 7.937 $\pm$ 0.0005 kg was used from a dry mass of 7.526 $\pm$ 0.0005 kg. Hence, the actual value of S_r in this experiment was 0.102 $\pm$ 0.003.

Lawn quartz: The calculated minimum mass of wet lawn quartz was 7.849 kg, when using a dry mass of 7.500 kg. In reality, a wet mass of 7.942 $\pm$ 0.0005 kg was used from a dry mass of 7.526 $\pm$ 0.0005 kg. Hence, the actual value of S_r in this experiment was 0.120 $\pm$ 0.004.

Joint sand: The calculated minimum mass of wet sand needed for each experiment had to be 8.051, when using a dry mass of 7.500 kg.

In reality, a wet mass of 8.250 ± 0.0005 kg was used from a dry mass of 7.565 ± 0.0005 kg. Hence, the actual value of S_r in this experiment was 0.125 ± 0.003.

Lawn sand: In reality, a wet mass of 8.118 ± 0.0005 kg was used from a dry mass of 7.530 ± 0.0005 kg. Hence, the actual value of S_r in this experiment was 0.107 ± 0.002.

Quartz sand: In reality, a wet mass of 8.140 ± 0.0005 kg was used from a dry mass of 7.519 ± 0.0005 kg. Hence, the actual value of S_r in this experiment was 0.113 ± 0.003.

B Rock analyzer

B.1 fully saturated data S_r = 1.000

Crushed marble stone: A wet mass of 0.219 ± 0.0005 kg was used from a dry mass of 0.200 ± 0.0005 kg. Hence, the actual value of S_r in this experiment was 1.356 ± 0.070.

Round/Quartz gravel: A wet mass of 0.180 ± 0.0005 kg was used from a dry mass of 0.154 ± 0.0005 kg. Hence, the actual value of S_r in this experiment was 1.000 ± 0.033.

Lawn quartz: A wet mass of 0.172 ± 0.0005 kg was used from a dry mass of 0.149 ± 0.0005 kg. Hence, the actual value of S_r in this experiment was 1.286 ± 0.053.

Joint sand: A wet mass of 0.279 ± 0.0005 kg was used from a dry mass of 0.264 ± 0.0005 kg. Hence, the actual value of S_r in this experiment was 1.016 ± 0.062.

Lawn sand: A wet mass of 0.244 ± 0.0005 kg was used from a dry mass of 0.201 ± 0.0005 kg. Hence, the actual value of S_r in this experiment was 1.118 ± 0.023.

Quartz sand: A wet mass of 0.300 ± 0.0005 kg was used from a dry mass of 0.282 ± 0.0005 kg. Hence, the actual value of S_r in this experiment was 2.252 ± 0.166.

B.2 Unsaturated data S_r = 0.500

Crushed marble stone: A wet mass of 0.209 ± 0.0005 kg was used from a dry mass of 0.201 ± 0.0005 kg. Hence, the actual value of S_r in this experiment was 0.592 ± 0.057.

Round/Quartz gravel: A wet mass of 0.166 ± 0.0005 kg was used from a dry mass of 0.153 ± 0.0005 kg. Hence, the actual value of S_r in this experiment was 0.489 ± 0.028.

Lawn quartz: A wet mass of 0.161 ± 0.0005 kg was used from a dry mass of 0.149 ± 0.0005 kg. Hence, the actual value of S_r in this experiment was 0.671 ± 0.044.

Joint sand: A wet mass of 0.269 $\pm$ 0.0005 kg was used from a dry mass of 0.260 $\pm$ 0.0005 kg. Hence, the actual value of S_r in this experiment was 0.553 $\pm$ 0.047.

Lawn sand: A wet mass of 0.227 $\pm$ 0.0005 kg was used from a dry mass of 0.205 $\pm$ 0.0005 kg. Hence, the actual value of S_r in this experiment was 0.600 $\pm$ 0.021.

Quartz sand: A wet mass of 0.287 $\pm$ 0.0005 kg was used from a dry mass of 0.282 $\pm$ 0.0005 kg. Hence, the actual value of S_r in this experiment was 0.625 $\pm$ 0.100.

B.3   Unsaturated data $S_r = 0.100$

Crushed marble stone: A wet mass of 0.157 $\pm$ 0.0005 kg was used from a dry mass of 0.151 $\pm$ 0.0005 kg. Hence, the actual value of S_r in this experiment was 0.156 $\pm$ 0.018.

Round/Quartz gravel: A wet mass of 0.154 $\pm$ 0.0005 kg was used from a dry mass of 0.150 $\pm$ 0.0005 kg. Hence, the actual value of S_r in this experiment was 0.141 $\pm$ 0.025.

Lawn quartz: A wet mass of 0.150 $\pm$ 0.0005 kg was used from a dry mass of 0.147 $\pm$ 0.0005 kg. Hence, the actual value of S_r in this experiment was 0.156 $\pm$ 0.037.

Joint sand: A wet mass of 0.254 $\pm$ 0.0005 kg was used from a dry mass of 0.251 $\pm$ 0.0005 kg. Hence, the actual value of S_r in this experiment was 0.153 $\pm$ 0.036.

Lawn sand: A wet mass of 0.208 $\pm$ 0.0005 kg was used from a dry mass of 0.200 $\pm$ 0.0005 kg. Hence, the actual value of S_r in this experiment was 0.206 $\pm$ 0.018.

Quartz sand: A wet mass of 0.283 $\pm$ 0.0005 kg was used from a dry mass of 0.282 $\pm$ 0.0005 kg. Hence, the actual value of S_r in this experiment was 0.125 $\pm$ 0.089.

Figure 31 shows the pipe used for measurements and this represented a borehole.

C   Vista Clara DART probe: Operation and data processing instructions

C.1   Set up and operation of the Dart probe

The instructions below are a summary of the manual, so for a more detailed overview see [29].

1. Connect logging cable to DART probe and screw until tightened.
2. Connect the other end of logging cable to SENSOR port on control unit.
3. Connect field computer via data cable to USB port on control unit.
4. Connect battery to 12 V BATT port on control unit.
5. Place DART probe into sample i.e., borehole.
6. Turn on laptop and control unit.
7. Check system frequencies and diagnostics are functioning i.e., diagnostic ping.
8. Set well depth height and measuring increment to desired magnitudes.
9. Begin measurements.

Figure 31: The pipe used to demonstrate borehole conditions with dimensions: height= 1.120 ± 0.001 m and diameter 0.151 ± 0.001 m.

10. Upon completion of measurements turn off control unit and remove DART probe from sample i.e., borehole.

11. Dismantle apparatus in reverse order of steps 1-4.

C.2 Data processing after data collection

The instructions below are a summary of the manual, so for a more detailed overview see [29].

1. Open Dart Log Processing software (JavelinProPlus).
2. Select data file to analyse.
3. If the user wishes, select 'Remove Impulse Noise' to remove any noise that could affect the data.
4. It is not recommended to change any other parameters unless the user is very experienced with the software.
5. Acquire data regarding T_2, water content and hydraulic conductivity estimates.
6. Export data as MATLAB file or wellCAD which are the the two options.

D   NUCLEUSinv software
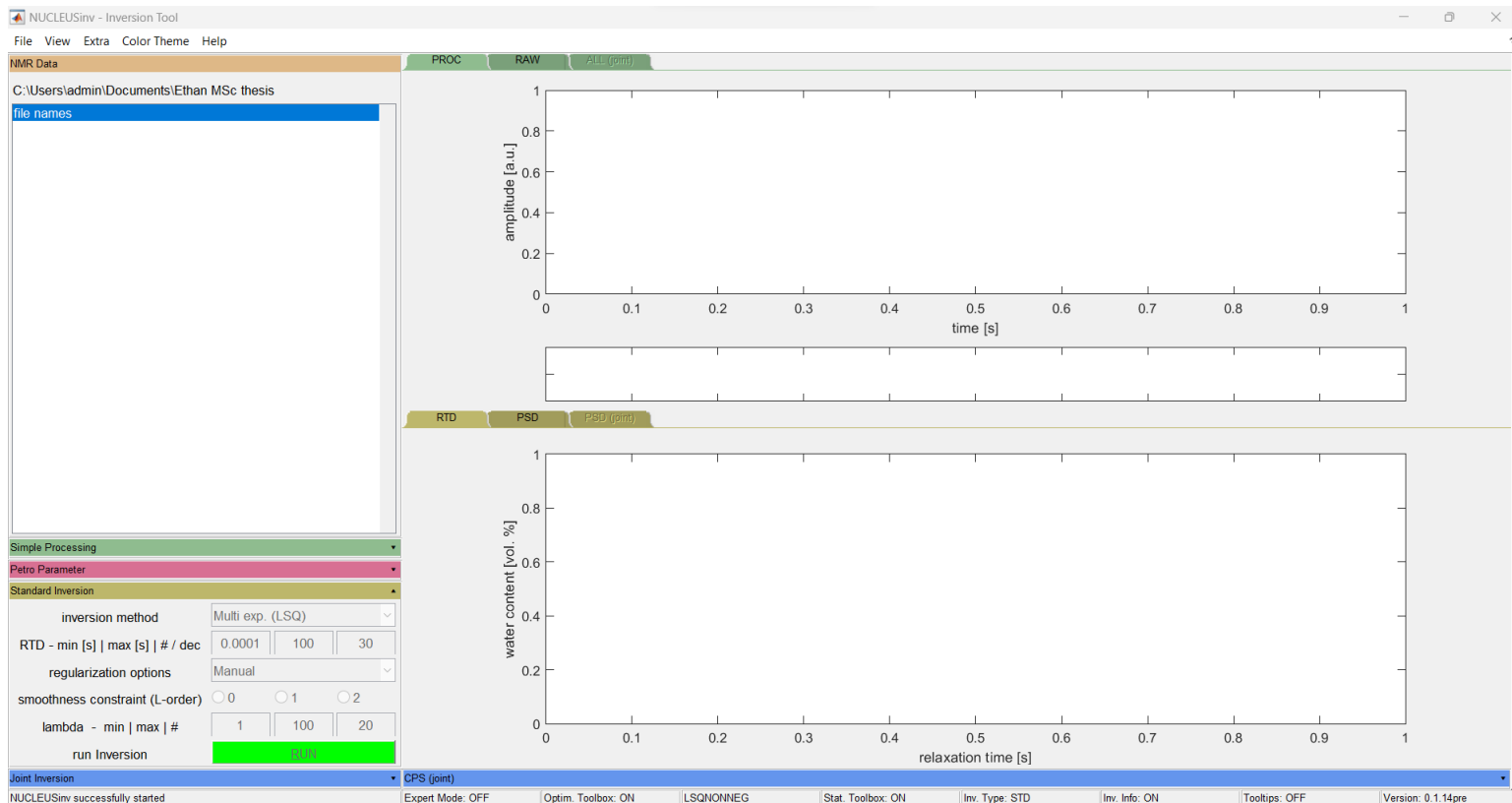
Figure 32: The inverse modelling part of the NUCLEUS software used, to produce the T_2 relaxation curves and pore-size distribution graphs for this thesis. This is a free open source software produced by Dr. Thomas Hiller [30].

The following instructions should be used only if the user wishes to use NUCLEUS via MATLAB,

and data from the DART probe. Before following the instructions below, install NUCLEUS and make sure it is in the 'path' in whatever folder you use for MATLAB. Other graphing software/ programs could be used to plot the T_2 and pore size distribution curves.

As mentioned before, there are no official instructions or manual for NUCLEUSinv (at the time of completion of this thesis). Therefore, I was not familiar with the software and had to become accustom to it. There is also information on [30] if the reader would like to learn more about NUCLEUS.

1. Open MATLAB and type into the terminal: startNUCLEUSinv, then click enter.
2. Click on: File ==> Import ==> Lab ==> Other ==> Dart, and select data file to analyse.
3. Select the depth height that you would like to analyze, e.g. 0.00 m or 0.25 m etc.
4. Select inversion method: Multiple exponents (Least-squares), Mono exponents or Several free exponents (The 'Multiple exponents' was used in this thesis).
5. After selecting 'Multiple exponents' as the inversion method, select 'Manual' for regularization option, and click 'RUN'.
6. On the right of these variables, the user should see two tabs aboce the bottom (white) panel, the tab named 'RTD' is for the T_2 relaxation curve and the tab named 'PSD' is for the pore-size distribution. The top panel in figure 32 shows the decay curve of the spin echoes.
7. Some constants can not be changed or should only be changed with more in depth knowledge of NMR data interpretation.

Acknowledgments